IEEE Open Journal of
Vehicular Technology

Received 25 May 2021; accepted 1 June 2021. Date of publication 8 June 2021;
date of current version 5 July 2021. The review of this article was arranged by Editor Jemin Lee.

Digital Object Identifier 10.1109/OJVT.2021.3087637

Joint Impact of Nodes Mobility and Imperfect Channel Estimates on the Secrecy Performance of Cognitive Radio Vehicular Networks Over Nakagami-*m* Fading Channels

ANSHUL PANDEY [1] (Member, IEEE), AND SUNEEL YADAV [2] (Member, IEEE)

[1]Secure Systems Research Center, Technology Innovation Institute, Abu Dhabi 9639, United Arab Emirates
[2]Department of Electronics and Communication Engineering, Indian Institute of Information Technology Allahabad, Prayagraj 211015, India

CORRESPONDING AUTHOR: ANSHUL PANDEY (e-mail: anshul@ssrc.tii.ae).

This work was supported by Secure Systems Research Center, Technology Innovation Institute, United Arab Emirates.

ABSTRACT This paper investigates the joint impact of nodes' mobility and imperfect channel estimates on the secrecy performance of an underlay cognitive radio vehicular network over Nakagami-*m* fading channels. Specifically, the secondary network consists of a single-antenna source vehicle, an N_{D}-antenna destination vehicle, and an N_{E}-antenna passive eavesdropper vehicle, whereas the primary network comprises of a single-antenna primary receiver vehicle. The time selective fading links arise due to nodes' mobility are modeled via first-order auto-regressive process, and the channel state information is estimated using linear minimum mean square error estimation method. Moreover, the transmit power of secondary source is constrained by both the interference threshold of the primary receiver and the maximum transmit power of secondary network. Under such a realistic scenario, we derive the analytical closed-form secrecy outage probability (SOP) and ergodic secrecy capacity expressions. Furthermore, we present asymptotic SOP analysis to obtain key insights into the system's secrecy diversity order. We also report several practical cases of interest to reveal valuable information about the system's secrecy behavior. Moreover, we illustrate the impacts of system/channel parameters, nodes' mobility, imperfect channel estimates, interference temperature limit, and the maximum available source power. Finally, the simulation studies corroborate our derived analytical findings.

INDEX TERMS Physical-layer security, cognitive radio vehicular networks, nodes' mobility, secrecy outage probability, ergodic secrecy capacity, imperfect channel estimates.

I. INTRODUCTION

With the proliferation of wireless technologies, the autonomous vehicles enabled with various wireless communication capabilities have transformed the simple transportation modes, e.g., cars, buses, into a novel paradigm of Internet of Vehicles (IoV) infrastructures [1]. IoV aims to enhance the performance of vehicular networks, which include various modes, such as, vehicle-to-vehicle (V2V), vehicle-to-infrastructure (V2I), vehicle-to-pedestrian (V2P), vehicle-to-network (V2N), and vehicle-to-everything (V2X) communications. Such vehicular networks are expected to empower an era of intelligent transportation systems (ITS) to provide better traffic management, efficient resource utilization, and an enriched infotainment and personal experiences to the users on the move [2]. Because of the lucrative services offered by such networks, they can play an integral role in the upcoming fifth generation and beyond communication networks [3], [4]. Since, such networks are engaged in both the real-time and non-real time services, and are having decentralized nature and heterogeneity in their characteristics, they may suffer from various issues in the form of security, mobility, and channel estimation [5], [6]. Moreover, such vehicular networks

also witnessed a huge surge in the wireless data traffic over the limited spectrum allocated for the communication [7].

Cognitive radio technology has emerged as a potential solution to resolve the spectrum scarcity issues in vehicular networks by allowing opportunistic spectrum sensing and hopping [8], also termed as cognitive radio vehicular networks (CRVNs). Since, bulk of the traffic will be transmitted over the wireless channel, therefore the wireless transmission in CRVNs is more vulnerable to security threats, such as, jamming and eavesdropping, due to the open wireless medium and dynamic nature of cognitive radios. Traditionally, security in wireless communications mainly depends on the encryption techniques in upper layer, such as, advanced encryption standard and data encryption standard, which require a powerful computational processing. However, these techniques may not be efficient owing to the heterogeneous, dynamic, and decentralized characteristics inhibited by such networks [9], [10]. Recently, physical layer security (PHY-security) has emerged as an attractive option to secure the wireless communications, as it exploits the inherent random behavior of the physical channel (multipath fading, interference, propagation delay etc.) and uses various coding, signal design, and signal processing techniques to realize the key-less secure transmissions [11], [12]. On the other hand, the channel becomes time selective due to the nodes' mobility or the Doppler spread effect, which will impose several challenges on CRVNs. Also, channel estimation errors while estimating the channel state information is also a major issue for such networks. Particularly, PHY-security in CRVNs is quite challenging under the combined effects of imperfect channel estimates and nodes' mobility, which is the main focus of this paper.

A. RELATED WORKS

The PHY-security performance for non-cognitive communication networks has been studied thoroughly in the literature [13]–[22]. Under the cognitive radio framework, several efforts have been made to investigate the PHY-security performance in the literature (see [23]–[36] and the references therein). In particular, the authors in [23] have exploited the benefits of multi-user diversity to secure the cognitive radio networks (CRNs) in the presence of multiple eavesdroppers. The authors in [24] have studied the benefits of multiple antennas on the security performance of CRNs. Moreover, the authors in [25] have investigated the security performance of cognitive relay networks under Rayleigh fading. The authors in [26], [27] have analyzed the impact of relay diversity on the security performance under Rayleigh fading. Furthermore, PHY-security performance of CRNs under Nakagami-*m* fading channels has been investigated in [28], [29]. The authors in [30] have studied the PHY-security in cognitive relay networks with multiple eavesdroppers over Rayleigh fading. Recently, the secrecy performance of jamming based underlay CRNs has been evaluated in [31] over Nakagami-*m* fading channels. The authors in [32] have studied an artificial noise based energy efficient beamforming scheme for CRNs in the presence of multiple eavesdroppers over Rayleigh fading. Further, PHY-security in multiple-input-multiple-output CRNs with active eavesdropping has been studied over Rayleigh fading in [33]. Recently, the authors in [34] have investigated the tradeoff between reliability and security for non-orthogonal multiple access enabled cognitive radio networks. The authors in [35] have studied the secrecy performance of energy harvesting coupled cognitive radio networks. Furthermore, the authors in [36] have evaluated the performance of cognitive wiretap networks under $\alpha - \mu$ fading channels.

However, all the aforementioned studies [23]–[36] were limited to non-vehicular scenario, where the nodes are stationary. The PHY-security aspects for secure communications have been explored in several literature for non-cognitive vehicular communication networks [37]–[45] and for cognitive vehicular networks [46]–[48]. Moreover, it has to be emphasized that the channel between the nodes may become time-selective due to the mobility of the nodes. Furthermore, with time-selective links, it may be difficult for the destination tracking loops to estimate the channel perfectly, and hence causes channel estimation errors in the system. Therefore, it is important to consider the impact of node's mobility and imperfect channel estimates while evaluating the performance of vehicular communication networks. The works presented in [23]–[48] neither considered the impact of nodes' mobility nor the imperfect channel estimates. Recently, the authors in [49], [50] have evaluated the secrecy performance of multi-antenna communication networks with time-varying channels but under non-cognitive radio framework. Furthermore, the authors in [51] have investigated the secrecy performance of cognitive radio enabled V2I networks with nodes' mobility under Nakagami-*m* fading channels. Albeit, the efforts to exploit the benefits of PHY-security to secure CRVNs under the joint consideration of nodes' mobility and imperfect channel estimates are very limited. Very recently, the authors in [52] have made an effort to investigate the secrecy performance of CRVNs by considering the joint impact of nodes' mobility and imperfect channel estimates, but this work was limited under the consideration of i) single-antenna terminals case, ii) peak type of interference constraint at the primary receiver, iii) classical Rayleigh fading.

B. MOTIVATION

The evolution of vehicular communications paves the way for the ITS applications in fifth generation and beyond communication networks, as they are envisioned to interconnect human communication and modern day transportation [53]. However, vehicular networks suffer from various issues such as, security, spectrum scarcity, mobility, and the channel dynamics. To this end, several works have exploited the benefits of PHY-security for non-CRVNs in [37]–[45] and for CRVNs in [46]–[48]. Furthermore, the secrecy performance of CRVNs was studied under the impact of nodes' mobility in [51], and under the combined impact of impact of nodes' mobility and channel estimation error in [52]. However, the performance studies in [51] and [52] were investigated with

some relaxed constraints, which we have tried to incorporate in this work to thoroughly examine PHY-security in CRVNs. There are several differences between this paper and [51] and [52].

1) This paper is different from [51] in many aspects; i) the system model in [51] is different from this paper. In [51], the secondary source and the primary receiver are fixed terminals and the secondary destination and secondary eavesdropper are in motion, whereas this paper considers a V2V scenario in which all the primary and secondary nodes are moving vehicles, ii) this paper considers that the interference channel (i.e., between secondary source and primary receiver) is affected by both the time varying errors and imperfect channel estimates, while [51] assumes a perfect interference channel, iii) this paper investigates the joint impact of nodes' mobility and channel estimation errors, whereas [51] only considers the effect of nodes' mobility, iv) this paper considers the multi-antenna destination and eavesdropper nodes, whereas [51] assumes dual-antenna destination and eavesdropper nodes.
2) This paper has following differences from [52]; i) this paper assumes the combined power constraint of the interference on the primary network and the maximum transmit power constraint on the secondary network, whereas [52] considers a single power constraint of the interference on the primary network, ii) this paper assumes the multiple antennas at the secondary destination and secondary eavesdropper, whereas [52] considers single-antenna terminals, and iii) this paper investigates the system performance over Nakagami-*m* fading channels, whereas [52] studies the system performance over Rayleigh fading channels.

Therefore, these differences make the results of this paper fundamentally different from [51] and [52]. Nevertheless, to the best of authors' knowledge, this is the first work which thoroughly and comprehensively evaluates the secrecy performance of CRVNs by considering the joint impact of nodes' mobility and imperfect channel estimates with combined power constraint of the interference at primary receiver and maximum transmit power at the secondary source, and by employing the multiple antennas at the destination and eavesdropper vehicles, over Nakagami-*m* fading channels.

C. CONTRIBUTIONS

Based on the above discussion, it is clear that there is a lack of understanding about PHY-security performance in underlay CRVNs by taking the following into account; i) impact of nodes' mobility and imperfect channel estimates, ii) combined power constraint of the interference on the primary network and the maximum allowable transmission power at the secondary network, iii) multi-antenna secondary destination and eavesdropper, and iv) Nakagami-*m* fading channels. Therefore, this study thus i) poses various mathematical challenges and complications under the joint impact of nodes' mobility and imperfect channel estimates with combined power constraints, multi-antenna secondary receivers, and Nakagami-*m* fading channels, ii) results into the unique analytical findings which are reported first time in the literature to analyze PHY-security in CRVNs under such a realistic system set-up, and iii) lay the foundation for examining secrecy performance in CRVNs over more generalized and practical scenarios. Specifically, for the considered secure underlay CRVNs, we derive the secrecy outage probability (SOP), asymptotic SOP, and ergodic secrecy capacity (ESC) expressions in the presence of nodes' mobility and imperfect channel estimates over Nakagami-*m* fading channels. The key contributions of the paper can be summarized as follows.

1) By utilizing the i) first-order auto-regressive process to model all the time-varying channels (due to nodes' mobility) alongwith the linear minimum mean square error estimation method to estimate the channel state information, ii) combined power constraint of the interference at primary receiver and maximum transmit power at the secondary source, and iii) maximum ratio combining (MRC) at the multiple antennas equipped secondary destination and secondary eavesdropper, we first derive the instantaneous end-to-end signal-to-noise ratios (SNRs) at the destination and eavesdropper terminals for the considered underlay CRVNs.
2) Based on the derived instantaneous SNRs, we deduce the analytical closed-form expression for the SOP of the considered system under Nakagami-*m* fading channels. To get more information about the system's secrecy diversity order, we also derive the asymptotic SOP expressions under two scenarios, i.e., 1) when the average channel gain of the main link (between secondary source and secondary destination) goes to infinity with fixed average channel gain of the wiretap link (between secondary source and secondary eavesdropper), and 2) when the average channel gains of both the main and wiretap links go to infinity. From which, it is revealed that the system's secrecy performance degrades significantly due to the impact of nodes' mobility and imperfect channel estimates, irrespective of other involved channel/system parameters, and even reduces the system's secrecy diversity order to zero.
3) From the derived exact and asymptotic SOP expressions, we particularize some practical cases of interest; 1) Case 1: when all the nodes are mobile with perfect channel estimates, 2) Case 2: when all static nodes with imperfect channel estimates, and 3) Case 3: when all static nodes with perfect channel estimates. It is highlighted that the system's secrecy diversity order becomes zero under Case 1 and Case 2, regardless of the involved fading severity parameters and number of antennas. However, a full secrecy diversity order of $N_{\mathrm{D}}m_{\mathrm{SD}}$ can be achieved under Case 3, where N_{D} denotes the number of antennas at the destination and m_{SD} is the fading severity parameter for the main link. We also investigate the impact of the interference

temperature limit and the maximum available power at the source terminal on the system's SOP performance.

4) We then derive a tight novel expression for the ESC of the considered system under the combined impact of nodes' mobility and imperfect channel estimates over Nakagami-m fading channels.
5) Finally, we verify our derived theoretical findings via numerical and simulation results, and show the impact of i) nodes' mobility, ii) imperfect channel estimates, iii) fading severity parameters and average channel gains associated with the main link, wiretap link, and interference link (between secondary source and primary receiver), iv) number of antennas equipped at the destination and eavesdropper terminals, and v) interference threshold on the primary receiver and maximum allowable transmission power at secondary source, on the systems' secrecy performance.

The remainder of this paper is organized as follows. Section II describes our considered network setup. Section III provides exact and asymptotic SOP expressions. We also provide some practical cases of interest on the SOP analysis. An ESC expression is also derived. In Section IV, we present numerical and simulation results, followed by conclusions in Section V.

Notations: $\mathbb{E}[.]$ denotes the expectation operator, $[.]^{\mathrm{T}}$ denotes transpose operation, $[\cdot]^{\mathcal{H}}$ denotes conjugate transpose operation, $|\cdot|$ and $||\cdot||$ represent absolute value and Frobenius norm, respectively. $F_X(x)$ and $f_X(x)$ denote the cumulative distribution function (CDF) and the probability density function (PDF) of a random variable (RV) X. $\Gamma(x)$ is the complete Gamma function [60, eq. (8.310.1)], $\Gamma(n, x)$ is the upper incomplete Gamma function [60, eq. (8.350.2)], $\Upsilon(n, x)$ is the lower incomplete Gamma function [60, eq. (8.350.1)], $\Psi(\cdot, \cdot, \cdot)$ is the Tricomi confluent hypergeometric function [60, eq. (9.210.2)], and $\mathcal{G}_{p,q}^{m,n}(x|_{b_1,\ldots,b_q}^{a_1,\ldots,a_p})$ is the Meijer-$\mathcal{G}$ function [60, eq. (9.301)].

II. SYSTEM AND CHANNEL MODELS

We consider a secure CRVN as depicted in Fig. 1, wherein a secondary wiretap vehicular network operates in the spectral band licensed by a primary vehicular network in underlay mode. The primary system consists of a primary receiver vehicle (P), and the secondary wiretap network has a source vehicle (S), a destination vehicle (D), and an eavesdropper vehicle (E). We assume that E is passive in nature, and can pose threat to the security of the secondary network information by attempting to overhear the secondary transmissions. All the vehicles in both the secondary and primary networks are in motion, and the secondary transmission causes an interference to the primary network. We assume that the vehicles S and P are the single antenna terminals, while the vehicles D and E are equipped with N_{D} and N_{E} antennas, respectively. Moreover, the multiple antennas at D and E are assumed to be sufficiently apart with the spacing greater than half wavelength, and all the multiple antenna nodes

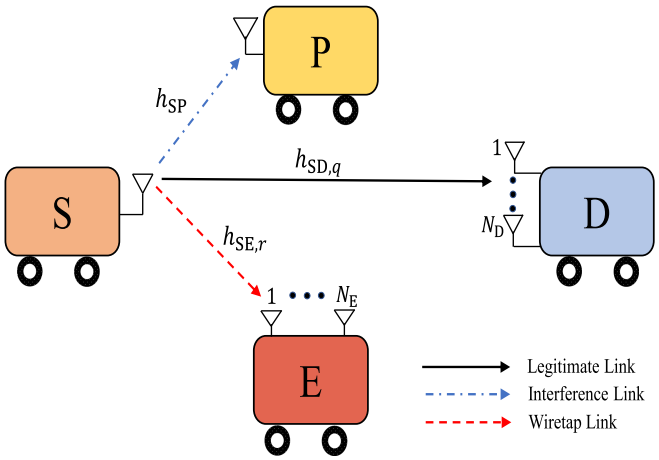

FIGURE 1. System model for the considered secure cognitive vehicular radio network.

experience a high azimuthal spread. Therefore, the multiple antennas at vehicles D and E are assumed to be uncorrelated [55], [56]. Furthermore, the vehicles in the network operate in half-duplex mode. The channels for all the links are assumed to undergo frequency-flat time-selective independent and identically distributed (i.i.d.) Nakagami-m fading.[1] Since S $\rightarrow$ D (main link) and S $\rightarrow$ E (wiretap link) channels form single-input-multiple-output (SIMO) links, therefore, the channel vectors for the links S $\rightarrow$ D and S $\rightarrow$ E can be denoted as $\mathbf{h}_{\mathrm{SD}} = [h_{\mathrm{SD},1}, h_{\mathrm{SD},2}, \cdots, h_{\mathrm{SD},N_{\mathrm{D}}}]^{\mathrm{T}}$ and $\mathbf{h}_{\mathrm{SE}} = [h_{\mathrm{SE},1}, h_{\mathrm{SE},2}, \cdots, h_{\mathrm{SE},N_{\mathrm{E}}}]^{\mathrm{T}}$, respectively. Moreover, the entries $h_{\mathrm{SD},q}, q \in \{1, 2, \ldots, N_{\mathrm{D}}\}$ and $h_{\mathrm{SE},r}, r \in \{1, 2, \ldots, N_{\mathrm{E}}\}$ are modeled as i.i.d. Nak($m_{\mathrm{SD}}, \Omega_{\mathrm{SD}}$) and Nak($m_{\mathrm{SE}}, \Omega_{\mathrm{SE}}$), respectively. As S and P are single-antenna terminals, thus, the channel coefficient for S $\rightarrow$ P link (interference link) is denoted by $h_{\mathrm{SP}} \sim$ Nak($m_{\mathrm{SP}}, \Omega_{\mathrm{SP}}$). In addition, the additive white Gaussian noise (AWGN) at each node is modeled with zero mean and variance N_0.

A. MODELING OF NODES' MOBILITY AND IMPERFECT CHANNEL ESTIMATES

As is well known that the fading links are time-selective due to the effect of nodes' mobility, therefore, we use the first-order auto-regressive (AR1) process [54] to model and represent $\mathbf{h}_{\mathrm{S}\iota}$, for $\iota \in \{\mathrm{D}, \mathrm{E}\}$ and h_{SP} as

$$\mathbf{h}_{\mathrm{S}\iota} = \rho_{\mathrm{S}\iota}\bar{\mathbf{h}}_{\mathrm{S}\iota} + \sqrt{1 - \rho_{\mathrm{S}\iota}^2}\mathbf{h}_{e_{\mathrm{S}\iota}}, \tag{1}$$

[1] It is both theoretically and experimentally proved that Nakagami-m fading model is suitable for a wide range of application scenarios including vehicular communications. For instance, the experimental study in [57] showed that the Nakagami-m fading well describes the static and small-scale fading in V2V communications through Akaike's information criterion and the kolmogorov-Smirnov tests. The works in [58] showed that the Nakagami-m fading offers a good fit to the channel conditions for a millimeter wave networks for highway V2V communications. Also, such a fading scenario has been found suitable to model the V2V channel characteristics at 700 MHz band [59]. Motivated by this, we adopted Nakagami-m fading model over other generalized distributions, such as, $\alpha - \mu$ fading, $\alpha - \eta - \kappa - \mu$ fading, etc.

$$h_{\mathrm{SP}} = \rho_{\mathrm{SP}}\bar{h}_{\mathrm{SP}} + \sqrt{1-\rho_{\mathrm{SP}}^2}h_{e_{\mathrm{SP}}}, \tag{2}$$

respectively, where $\{\mathbf{h}_{\mathrm{S}\iota},\ h_{\mathrm{SP}}\}$and $\{\bar{\mathbf{h}}_{\mathrm{S}\iota}, \bar{h}_{\mathrm{SP}}\}$ are the channel gains during the transmission of the current and immediately previous information symbols, respectively. Moreover, $\mathbf{h}_{e_{\mathrm{S}\iota}}$, for $\iota \in \{\mathrm{D}, \mathrm{E}\}$, represent the time-varying vector component between $\mathrm{S} \to \iota$ link and can be modeled as i.i.d. $\mathcal{CN}(0,\ \Omega_{e_{\mathrm{S}\iota}}\mathbf{I}_{e_{\mathrm{S}\iota}})$. Also, $h_{e_{\mathrm{SP}}} \sim \mathcal{CN}(0, \Omega_{e_{\mathrm{SP}}})$ represents the time-varying component of $\mathrm{S} \to \mathrm{P}$ link. The duo of channel coefficients $\bar{\mathbf{h}}_{\mathrm{SD}}$ and $\mathbf{h}_{e_{\mathrm{SD}}}$, $\bar{\mathbf{h}}_{\mathrm{SE}}$ and $\mathbf{h}_{e_{\mathrm{SE}}}$, and $\bar{h}_{\mathrm{SP}}$ and $h_{e_{\mathrm{SP}}}$ are jointly Gaussian distributed with correlation coefficient $\rho_{\mathrm{S}\jmath} \in [0, 1]$, for $\jmath \in \{\mathrm{D}, \mathrm{E}, \mathrm{P}\}$. Using Jake's model, the correlation parameters can be modeled as $\rho_{\mathrm{S}\jmath} = J_0(\frac{2\pi f_c v_{\mathrm{S}\jmath}}{Rc})$, for $\jmath \in \{\mathrm{D}, \mathrm{E}, \mathrm{P}\}$, where $v_{\mathrm{S}\jmath}$ denotes the relative speed between the nodes S and $\jmath$, f_c is the carrier frequency, R is the code rate, c is speed of light, and $J_0(\cdot)$ denotes the zeroth-order Bessel function of the first kind [60].

In addition, channel estimation errors do exist in the system during the channel estimation process, which results into the imperfect channel estimates. Therefore, assuming linear minimum mean square error estimation process, we can model the estimated channel vector $\hat{\mathbf{h}}_{\mathrm{S}\iota}$, for $\iota \in \{\mathrm{D}, \mathrm{E}\}$ and channel gain $\hat{h}_{\mathrm{SP}}$ as

$$\bar{\mathbf{h}}_{\mathrm{S}\iota} = \hat{\mathbf{h}}_{\mathrm{S}\iota} + \mathbf{h}_{\epsilon_{\mathrm{S}\iota}}, \tag{3}$$

$$\bar{h}_{\mathrm{SP}} = \hat{h}_{\mathrm{SP}} + h_{\epsilon_{\mathrm{SP}}}, \tag{4}$$

where $\mathbf{h}_{\epsilon_{\mathrm{S}\iota}} \sim \mathcal{CN}(0, \Omega_{\epsilon_{\mathrm{S}\iota}}\mathbf{I}_{\epsilon_{\mathrm{S}\iota}})$ and $h_{\epsilon_{\mathrm{SP}}} \sim \mathcal{CN}(0, \Omega_{\epsilon_{\mathrm{SP}}})$ denote the estimation errors and are mutually independent and orthogonal from the estimated channels.

Now invoking (3) into (1), we can get the following relationship for $\mathbf{h}_{\mathrm{S}\iota}$, for $\iota \in \{\mathrm{D}, \mathrm{E}\}$, in the presence of nodes' mobility and imperfect channel estimates as

$$\begin{aligned}\mathbf{h}_{\mathrm{S}\iota} &= \rho_{\mathrm{S}\iota}(\hat{\mathbf{h}}_{\mathrm{S}\iota} + \mathbf{h}_{\epsilon_{\mathrm{S}\iota}}) + \sqrt{1-\rho_{\mathrm{S}\iota}^2}\mathbf{h}_{e_{\mathrm{S}\iota}} \\ &= \rho_{\mathrm{S}\iota}\hat{\mathbf{h}}_{\mathrm{S}\iota} + \mathbf{w}_{\mathrm{S}\iota},\end{aligned} \tag{5}$$

where $\mathbf{w}_{\mathrm{S}\iota} = \rho_{\mathrm{S}\iota}\mathbf{h}_{\epsilon_{\mathrm{S}\iota}} + \sqrt{1-\rho_{\mathrm{S}\iota}^2}\mathbf{h}_{e_{\mathrm{S}\iota}}$ with variance $\Omega_{w_{\mathrm{S}\iota}} = \rho_{\mathrm{S}\iota}^2\Omega_{\epsilon_{\mathrm{S}\iota}} + (1-\rho_{\mathrm{S}\iota}^2)\Omega_{e_{\mathrm{S}\iota}}$.

Likewise, invoking (4) into (2), we can express the interference channel gain h_{SP} as

$$h_{\mathrm{SP}} = \rho_{\mathrm{SP}}\hat{h}_{\mathrm{SP}} + w_{\mathrm{SP}}, \tag{6}$$

where $w_{\mathrm{SP}} = \rho_{\mathrm{SP}}h_{\epsilon_{\mathrm{SP}}} + \sqrt{1-\rho_{\mathrm{SP}}^2}h_{e_{\mathrm{SP}}}$ with variance $\Omega_{w_{\mathrm{SP}}} = \rho_{\mathrm{SP}}^2\Omega_{\epsilon_{\mathrm{SP}}} + (1-\rho_{\mathrm{SP}}^2)\Omega_{e_{\mathrm{SP}}}$.

B. INSTANTANEOUS END-TO-END SNRS

In the secondary network, S sends confidential information carrying signal x_s of unit energy with power P_{S} to D. A passive secondary vehicle E in the close vicinity attempts to intercept this secret information. Further, with the time varying fading channels and imperfect channel estimates, the received signal vector $\mathbf{Y}_\iota$ at node ι, for $\iota = \{\mathrm{D}, \mathrm{E}\}$ can be given as

$$\begin{aligned}\mathbf{Y}_\iota = &\underbrace{\sqrt{P_{\mathrm{S}}}\rho_{\mathrm{S}\iota}\hat{\mathbf{h}}_{\mathrm{S}\iota}x_s}_{\text{desired information signal}} + \underbrace{\sqrt{P_{\mathrm{S}}}\rho_{\mathrm{S}\iota}\mathbf{h}_{\epsilon_{\mathrm{S}\iota}}x_s}_{\text{noise from imperfect channel estimates}} \\ &+ \underbrace{\sqrt{P_{\mathrm{S}}}\sqrt{1-\rho_{\mathrm{S}\iota}^2}\mathbf{h}_{e_{\mathrm{S}\iota}}x_s}_{\text{noise due to nodes' mobility}} + \underbrace{\mathbf{n}_\iota}_{\text{white noise}},\end{aligned} \tag{7}$$

where $\mathbf{n}_\iota = [n_{\iota,1}, n_{\iota,2}, \cdots, n_{\iota,N_\iota}]^T$ represents noise vector at the receiver $\iota = \{\mathrm{D}, \mathrm{E}\}$, whose entries $n_{\iota,\jmath}$, $\jmath \in \{1, 2, \cdots, N_\iota\}$ are modeled as $\mathcal{CN}(0, N_0)$.

Moreover, by applying MRC scheme at D and E, we can express (7) as

$$\begin{aligned}\mathbf{R}_\iota &= \mathbf{B}_\iota^{\mathcal{H}}\mathbf{Y}_\iota \\ &= \sqrt{P_{\mathrm{S}}}\rho_{\mathrm{S}\iota}\mathbf{B}_\iota^{\mathcal{H}}\hat{\mathbf{h}}_{\mathrm{S}\iota}x_s + \sqrt{P_{\mathrm{S}}}\rho_{\mathrm{S}\iota}\mathbf{B}_\iota^{\mathcal{H}}\mathbf{h}_{\epsilon_{\mathrm{S}\iota}}x_s \\ &\quad + \sqrt{P_{\mathrm{S}}}\sqrt{1-\rho_{\mathrm{S}\iota}^2}\mathbf{B}_\iota^{\mathcal{H}}\mathbf{h}_{e_{\mathrm{S}\iota}}x_s + \mathbf{B}_\iota^{\mathcal{H}}\mathbf{n}_\iota,\end{aligned} \tag{8}$$

where $\mathbf{B}_\iota = \frac{\hat{\mathbf{h}}_{\mathrm{S}\iota}}{||\hat{\mathbf{h}}_{\mathrm{S}\iota}||}$ is $N_\iota \times 1$ received beamforming vector at $\iota = \{\mathrm{D}, \mathrm{E}\}$. In addition, we make the reasonable assumption that the noise samples across the different antennas are independent, i.e., $\mathbb{E}\{n_{\iota,u}n_{\iota,v}^*\} = 0$ for $u \neq v$ and $\iota = \{\mathrm{D}, \mathrm{E}\}$. This can also be expressed using the covariance matrix $\mathbb{R}_{\mathbf{n}_\iota}$, for $\iota = \{\mathrm{D}, \mathrm{E}\}$, as $\mathbb{R}_{\mathbf{n}_\iota} = \mathbb{E}\{n_{\iota,u}n_{\iota,v}^*\} = N_0\mathbf{I}_{N_\iota}$. Furthermore, after some simplifications, the instantaneous end-to-end SNRs at the terminals D and E, respectively, as

$$\Lambda_{\mathrm{D}} = \frac{P_{\mathrm{S}}\rho_{\mathrm{SD}}^2\hat{Y}}{P_{\mathrm{S}}\rho_{\mathrm{SD}}^2\Omega_{\epsilon_{SD}} + P_{\mathrm{S}}(1-\rho_{\mathrm{SD}}^2)\Omega_{e_{\mathrm{SD}}} + N_0}, \tag{9}$$

$$\Lambda_{\mathrm{E}} = \frac{P_{\mathrm{S}}\rho_{\mathrm{SE}}^2\hat{Z}}{P_{\mathrm{S}}\rho_{\mathrm{SE}}^2\Omega_{\epsilon_{\mathrm{SE}}} + P_{\mathrm{S}}(1-\rho_{\mathrm{SE}}^2)\Omega_{e_{\mathrm{SE}}} + N_0}, \tag{10}$$

where $\hat{Y} = ||\hat{\mathbf{h}}_{\mathrm{SD}}||^2 \triangleq \sum_{l=1}^{N_{\mathrm{D}}} |\hat{h}_{\mathrm{SD}_l}|^2$ and $\hat{Z} = ||\hat{\mathbf{h}}_{\mathrm{SE}}||^2 \triangleq \sum_{k=1}^{N_{\mathrm{E}}} |\hat{h}_{\mathrm{SE}_k}|^2$.

Moreover, there is a constraint on the transmit power of S, so that the interference imposed on the primary receiver P is below the pre-determined tolerable interference limit $\mathcal{Q}$. This indicates that the instantaneous power at S should be constrained as $\mathbb{E}\{|(\rho_{\mathrm{SP}}\hat{h}_{\mathrm{SP}} + w_{\mathrm{SP}})x_s|^2\} \leq \mathcal{Q}$ and accordingly, $P_{\mathrm{S}} = \frac{\mathcal{Q}}{\rho_{\mathrm{SP}}^2|\hat{h}_{\mathrm{SP}}|^2 + \rho_{\mathrm{SP}}^2\Omega_{\epsilon_{\mathrm{SP}}} + (1-\rho_{\mathrm{SP}}^2)\Omega_{e_{\mathrm{SP}}}}$. Also, if S is power limited terminal, then the maximum power available with S is $P_{\max}$. Therefore, the transmit power at S can be expressed as

$$P_{\mathrm{S}} = \min\left(\frac{\mathcal{Q}}{\rho_{\mathrm{SP}}^2|\hat{h}_{\mathrm{SP}}|^2 + \Omega_{w_{SP}}}, P_{\max}\right). \tag{11}$$

Furthermore, with the help of (9), (10), and (11), we can finally express the instantaneous end-to-end SNRs at D and E as

$$\Lambda_{\mathrm{D}} = \min\left(\frac{\varrho_1\rho_{\mathrm{SD}}^2}{\rho_{\mathrm{SP}}^2\hat{X} + \Omega_{w_{\mathrm{SP}}} + \varrho_1\Omega_{w_{\mathrm{SD}}}}, \frac{\varrho_2\rho_{\mathrm{SD}}^2}{\varrho_2\Omega_{w_{\mathrm{SD}}} + 1}\right)\hat{Y}, \tag{12}$$

$$\Lambda_{\mathrm{E}} = \min\left(\frac{\varrho_1\rho_{\mathrm{SE}}^2}{\rho_{\mathrm{SP}}^2\hat{X}+\Omega_{w_{\mathrm{SP}}}+\varrho_1\Omega_{w_{\mathrm{SE}}}}, \frac{\varrho_2\rho_{\mathrm{SE}}^2}{\varrho_2\Omega_{w_{\mathrm{SE}}}+1}\right)\hat{Z}, \tag{13}$$

respectively, where $\hat{X} = |\hat{h}_{\mathrm{SP}}|^2$. Also, $\varrho_1 \triangleq \frac{\mathcal{Q}}{N_0}$ and $\varrho_2 \triangleq \frac{P_{\max}}{N_0}$ are denoted as the average transmit SNRs.

Moreover, the channel capacities pertaining to S $\rightarrow$ D link (i.e., main channel) and S $\rightarrow$ E link (i.e., wiretap channel) are expressed as $\mathbb{C}_{\mathrm{D}} = \log_2(1+\Lambda_{\mathrm{D}})$ and $\mathbb{C}_{\mathrm{E}} = \log_2(1+\Lambda_{\mathrm{E}})$, respectively. Therefore, the secrecy capacity of the wireless transmission can be given as the capacity difference between the main channel and that of the wiretap channel, i.e., $\mathbb{C}_{\mathrm{sec}}(\Lambda_{\mathrm{D}}, \Lambda_{\mathrm{E}}) = \max[\mathbb{C}_{\mathrm{D}} - \mathbb{C}_{\mathrm{E}}, 0]$.

C. PRELIMINARIES

Under Nakagami-m fading channels, the CDF and the PDF of $\hat{X} = |\hat{h}_{\mathrm{SP}}|^2$ are given as $F_{\hat{X}}(y) = \frac{1}{\Gamma(m_{\mathrm{SP}})}\Upsilon(m_{\mathrm{SP}}, \frac{m_{\mathrm{SP}}}{\Omega_{\mathrm{SP}}}y)$ and $f_{\hat{X}}(y) = \frac{1}{\Gamma(m_{\mathrm{SP}})}(\frac{m_{\mathrm{SP}}}{\Omega_{\mathrm{SP}}})^{m_{\mathrm{SP}}}y^{m_{\mathrm{SP}}-1}\mathrm{e}^{-\frac{m_{\mathrm{SP}}}{\Omega_{\mathrm{SP}}}y}$, respectively. It should also be noted that the summation of a large number of Gamma RV also follows Gamma distribution. Consequently, the CDF and PDF of $\hat{Y} = \sum_{l=1}^{N_{\mathrm{D}}}|\hat{h}_{\mathrm{SD}_l}|^2$ and $\hat{Z} = \sum_{k=1}^{N_{\mathrm{E}}}|\hat{h}_{\mathrm{SD}_k}|^2$ can be expressed as $F_{\kappa}(y) = \frac{1}{\Gamma(m_{\kappa_1}\kappa_2)}\Upsilon(m_{\kappa_1}\kappa_2, \frac{m_{\kappa_1}}{\Omega_{\kappa_1}}y)$ and $f_{\kappa}(y) = \frac{1}{\Gamma(m_{\kappa_1}\kappa_2)}(\frac{m_{\kappa_1}}{\Omega_{\kappa_1}})^{m_{\kappa_1}\kappa_2}y^{m_{\kappa_1}\kappa_2-1}\mathrm{e}^{-\frac{m_{\kappa_1}}{\Omega_{\kappa_1}}y}$, respectively, where $(\kappa, \kappa_1, \kappa_2) \in \{(\hat{Y}, \mathrm{SD}, N_{\mathrm{D}}), (\hat{Z}, \mathrm{SE}, N_{\mathrm{E}})\}$. These CDFs and PDFs will help us to perform the secrecy performance analysis of the considered system in what follows.

III. PERFORMANCE ANALYSIS

This section quantizes the secrecy performance of the considered CRVN in terms of the exact SOP and asymptotic SOP under Nakagami-m fading channels. Furthermore, to get more insights upon the impact of nodes' mobility and imperfect channel estimates on the secrecy performance, we present some special cases of interest. We also derive a novel tight expression for the ESC of the considered system.

A. EXACT SOP ANALYSIS

The SOP quantizes the network secrecy performance in the probabilistic terms by informing when the achievable secrecy capacity is less than a predefined secrecy rate $\mathcal{R}_s$ (in bps/Hz). Mathematically, the SOP can be expressed as $\mathcal{P}_{\mathrm{out}}^{\mathrm{sec}} = \Pr[\max\{\mathbb{C}_{\mathrm{D}} - \mathbb{C}_{\mathrm{E}}, 0\} < \mathcal{R}_s]$. Now, we can see that for the case when $\mathbb{C}_{\mathrm{D}} \leq \mathbb{C}_{\mathrm{E}}$, $\mathcal{P}_{\mathrm{out}}^{\mathrm{sec}} = 1$, which implies that the secondary network security is always compromised. Therefore, we focus our attention to investigate the SOP for the case when $\mathbb{C}_{\mathrm{D}} > \mathbb{C}_{\mathrm{E}}$, and consequently, the SOP can be represented as

$$\begin{aligned}\mathcal{P}_{\mathrm{out}}^{\mathrm{sec}} &= \Pr\left[\mathbb{C}_{\mathrm{D}} - \mathbb{C}_{\mathrm{E}} < \mathcal{R}_s\right] \\ &= \Pr\left[\frac{1+\Lambda_{\mathrm{D}}}{1+\Lambda_{\mathrm{E}}} < \eta\right],\end{aligned} \tag{14}$$

where $\eta = 2^{\mathcal{R}_s}$ denotes the secrecy target threshold. Invoking (12) and (13) into (14), we can express the SOP, $\mathcal{P}_{\mathrm{out}}^{\mathrm{sec}}(\eta)$, as

$$\mathcal{P}_{\mathrm{out}}^{\mathrm{sec}}(\eta) = \Pr\left[\frac{1+\min\left(\frac{\varrho_1\rho_{\mathrm{SD}}^2}{\rho_{\mathrm{SP}}^2\hat{X}+\Omega_{w_{\mathrm{SP}}}+\varrho_1\Omega_{w_{\mathrm{SD}}}}, \frac{\varrho_2\rho_{\mathrm{SD}}^2}{\varrho_2\Omega_{w_{\mathrm{SD}}}+1}\right)\hat{Y}}{1+\min\left(\frac{\varrho_1\rho_{\mathrm{SE}}^2}{\rho_{\mathrm{SP}}^2\hat{X}+\Omega_{w_{\mathrm{SP}}}+\varrho_1\Omega_{w_{\mathrm{SE}}}}, \frac{\varrho_2\rho_{\mathrm{SE}}^2}{\varrho_2\Omega_{w_{\mathrm{SE}}}+1}\right)\hat{Z}} < \eta\right], \tag{15}$$

which can be then expressed after some algebraic manipulations as

$$\begin{aligned}\mathcal{P}_{\mathrm{out}}^{\mathrm{sec}}(\eta) = &\underbrace{\Pr\left[\frac{1+\frac{\varrho_1\rho_{\mathrm{SD}}^2\hat{Y}}{\rho_{\mathrm{SP}}^2\hat{X}+\Omega_{w_{\mathrm{SP}}}+\varrho_1\Omega_{w_{\mathrm{SD}}}}}{1+\frac{\varrho_1\rho_{\mathrm{SE}}^2\hat{Z}}{\rho_{\mathrm{SP}}^2\hat{X}+\Omega_{w_{\mathrm{SP}}}+\varrho_1\Omega_{w_{\mathrm{SE}}}}} < \eta, \hat{X} > c_1\right]}_{\triangleq\, \mathcal{P}_{\mathrm{out},1}^{\mathrm{sec}}(\eta)} \\ &+ \underbrace{\Pr\left[\frac{1+\frac{\varrho_2\rho_{\mathrm{SD}}^2\hat{Y}}{\varrho_2\Omega_{w_{\mathrm{SD}}}+1}}{1+\frac{\varrho_2\rho_{\mathrm{SE}}^2\hat{Z}}{\varrho_2\Omega_{w_{\mathrm{SE}}}+1}} < \eta, \hat{X} < c_1\right]}_{\triangleq\, \mathcal{P}_{\mathrm{out},2}^{\mathrm{sec}}(\eta)},\end{aligned} \tag{16}$$

where $c_1 = (\frac{\varrho_1}{\varrho_2} - \Omega_{w_{\mathrm{SP}}})\frac{1}{\rho_{\mathrm{SP}}^2}$. Furthermore, by simplifying (16), we can obtain the analytical closed-form expression for the SOP as presented in Theorem 1.

Theorem 1: The SOP, $\mathcal{P}_{\mathrm{sec}}^{\mathrm{out}}(\eta)$, of the considered CRVN in the presence of nodes' mobility and imperfect channel estimates over Nakagami-m fading channels can be given as

$$\mathcal{P}_{\mathrm{out}}^{\mathrm{sec}}(\eta) = \mathcal{P}_{\mathrm{out},1}^{\mathrm{sec}}(\eta) + \mathcal{P}_{\mathrm{out},2}^{\mathrm{sec}}(\eta), \tag{17}$$

where $\mathcal{P}_{\mathrm{out},1}^{\mathrm{sec}}(\eta)$ and $\mathcal{P}_{\mathrm{out},2}^{\mathrm{sec}}(\eta)$ are expressed, respectively, as

$$\begin{aligned}\mathcal{P}_{\mathrm{out},1}^{\mathrm{sec}}(\eta) = 1 &- \frac{\Upsilon(m_{\mathrm{SP}}, \frac{m_{\mathrm{SP}}}{\Omega_{\mathrm{SP}}}c_1)}{\Gamma(m_{\mathrm{SP}})} \\ &- \Xi\Psi\Bigg(u_2+u_3+u_4+1, u_2+u_3+u_4-N_{\mathrm{E}}m_{\mathrm{SE}} \\ &- u_1+2, \left(\frac{\beta_2}{\beta_1}+c_1\right)\left[\frac{m_{\mathrm{SD}}(\eta-1)}{\Omega_{\mathrm{SD}}\varrho_1\alpha_1} + \frac{m_{\mathrm{SP}}}{\Omega_{\mathrm{SP}}}\right]\Bigg),\end{aligned} \tag{18}$$

$$\begin{aligned}\mathcal{P}_{\mathrm{out},2}^{\mathrm{sec}}(\eta) = &\Bigg[1 - \sum_{m=0}^{N_{\mathrm{D}}m_{\mathrm{SD}}-1}\sum_{u_5=0}^{m}\binom{m}{u_5}\frac{1}{m!}\left(\frac{m_{\mathrm{SD}}}{\Omega_{\mathrm{SD}}}\right)^m\left(\frac{m_{\mathrm{SE}}}{\Omega_{\mathrm{SE}}}\right)^{N_{\mathrm{E}}m_{\mathrm{SE}}} \\ &\times \frac{\Gamma(N_{\mathrm{E}}m_{\mathrm{SE}}+u_5)}{\Gamma(N_{\mathrm{E}}m_{\mathrm{SE}})}\frac{\xi_1^m\mathrm{e}^{-\frac{m_{\mathrm{SD}}(\eta-1)\xi_1}{\Omega_{\mathrm{SD}}\varrho_2\rho_{\mathrm{SD}}^2}}}{\left(\frac{m_{\mathrm{SD}}\eta\alpha_2\xi_1}{\Omega_{\mathrm{SD}}\alpha_1\xi_2}+\frac{m_{\mathrm{SE}}}{\Omega_{\mathrm{SE}}}\right)^{N_{\mathrm{E}}m_{\mathrm{SE}}+u_5}} \\ &\times \left(\frac{\eta-1}{\varrho_2\rho_{\mathrm{SD}}^2}\right)^{m-u_5}\left(\frac{\eta\alpha_2}{\alpha_1\xi_2}\right)^{u_5}\Bigg]\left[\frac{\Upsilon\left(m_{\mathrm{SP}}, \frac{m_{\mathrm{SP}}}{\Omega_{\mathrm{SP}}}c_1\right)}{\Gamma(m_{\mathrm{SP}})}\right],\end{aligned} \tag{19}$$

with $\theta_1 = \frac{\Omega_{w_{SP}}+\varrho_1\Omega_{w_{SD}}}{\rho_{SP}^2}$, $\theta_2 = \frac{\Omega_{w_{SP}}+\varrho_1\Omega_{w_{SE}}}{\rho_{SP}^2}$, $\alpha_1 = \frac{\rho_{SD}^2}{\rho_{SP}^2}$, $\alpha_2 = \frac{\rho_{SE}^2}{\rho_{SP}^2}$, $\xi_1 = \varrho_2\Omega_{w_{SD}}+1$, $\xi_2 = \varrho_2\Omega_{w_{SE}}+1$, $\beta_1 = m_{SD}\eta\alpha_2\Omega_{SE}+m_{SE}\Omega_{SD}\alpha_1$, $\beta_2 = m_{SD}\eta\alpha_2\Omega_{SE}\theta_1 + m_{SE}\theta_2\Omega_{SD}\alpha_1$, and

$$\begin{aligned}\Xi = {} & \frac{\left(\frac{m_{SE}}{\Omega_{SE}}\right)^{N_E m_{SE}}\left(\frac{m_{SP}}{\Omega_{SP}}\right)^{m_{SP}}}{\Gamma(N_E m_{SE})\Gamma(m_{SP})}\sum_{w=0}^{N_D m_{SD}-1}\sum_{u_1=0}^{w}\sum_{u_2=0}^{w}\sum_{u_3=0}^{m_{SP}-1}\sum_{u_4=0}^{N_E m_{SE}} \\ & \times \frac{\left(\frac{m_{SD}}{\Omega_{SD}}\right)^{w}}{w!}\binom{w}{u_1}\binom{w}{u_2}\binom{m_{SP}-1}{u_3}\binom{N_E m_{SE}}{u_4}(\eta\alpha_2\alpha_1)^{u_1} \\ & \times \alpha_1^{N_E m_{SE}-w}(\theta_2+c_1)^{N_E m_{SE}-u_4}\Gamma(N_E m_{SE}+u_1) \\ & \times c_1^{m_{SP}-1-u_3}(\theta_1+c_1)^{w-u_2}\Gamma(u_2+u_3+u_4+1) \\ & \times \left(\frac{\beta_2}{\beta_1}+c_1\right)^{u_2+u_3+u_4-N_E m_{SE}-u_1+1} \\ & \times \left(\frac{\Omega_{SD}\Omega_{SE}}{\beta_1}\right)^{N_E m_{SE}+u_1}\left(\frac{\eta-1}{\varrho_1}\right)^{w-u_1} \\ & \times \mathrm{e}^{-\left(\frac{m_{SD}(\eta-1)\theta_1}{\Omega_{SD}\varrho_1\alpha_1}+\frac{m_{SD}c_1(\eta-1)}{\Omega_{SD}\varrho_1\alpha_1}+\frac{m_{SP}c_1}{\Omega_{SP}}\right)}. \end{aligned} \tag{20}$$

Proof: See Appendix A for the detailed derivation. ■

Remark 1: It should be noted that the SOP expression in (17) comprises of finite summations, complete and lower incomplete gamma functions, exponential functions, and the Tricomi confluent hypergeometric function. These functions mainly contain the channel/system parameters, such as, average channel gains (Ω_{SD}, Ω_{SE}, and Ω_{SP}), number of receive antennas (N_D and N_E), fading severity parameters (m_{SD}, m_{SE}, and m_{SP}), channel estimation errors ($\Omega_{\epsilon_{SD}}$, $\Omega_{\epsilon_{SE}}$, and $\Omega_{\epsilon_{SP}}$), time varying errors ($\Omega_{e_{SD}}$, $\Omega_{e_{SE}}$, and $\Omega_{e_{SP}}$), correlation coefficients (ρ_{SD}, ρ_{SE}, and ρ_{SP}), secrecy target rate ($\mathcal{R}_s$), and transmit SNRs (ϱ_1 and ϱ_2), and can easily be evaluated using Mathematica computational software. Consequently, the SOP can readily be evaluated for various involved channel/system parameters, which is demonstrated numerically in Section IV.

Remark 2: The SOP expression presented in (17) can be reduced to [52, eq. (16)] for the case when $m_{SD} = m_{SE} = m_{SP} = 1$ (i.e., Rayleigh fading channels), $N_D = N_E = 1$ (i.e., single-antenna destination and eavesdropper terminals), and $P_S = \frac{\mathcal{Q}}{\rho_{SP}^2|\hat{h}_{SP}|^2+\Omega_{w_{SP}}}$ (i.e., single power constraint of the interference on the primary receiver). This can be explained as follows; by considering the case $\frac{\mathcal{Q}}{\rho_{SP}^2|\hat{h}_{SP}|^2+\Omega_{w_{SP}}} < P_{\max}$ from (11), the SOP in (15) can be expressed as $\mathcal{P}_{out}^{sec}(\eta) = \Pr\left[\frac{1+\frac{\varrho_1\rho_{SD}^2\hat{Y}}{\rho_{SP}^2\hat{X}+\Omega_{w_{SP}}+\varrho_1\Omega_{w_{SD}}}}{1+\frac{\varrho_1\rho_{SE}^2\hat{Z}}{\rho_{SP}^2\hat{X}+\Omega_{w_{SP}}+\varrho_1\Omega_{w_{SE}}}} < \eta\right]$, which can be simplified with the help of [60, eqs. (3.351.3)] and [61, eq. (2.3.6.9)] to obtain [52, eq. (16)] for $m_{SD} = m_{SE} = m_{SP} = 1$ and $N_D = N_E = 1$. Therefore, the SOP analysis presented in this work can be treated as a generalization of [52].

B. ASYMPTOTIC SOP ANALYSIS

To reveal the impact of various involved system/channel parameters on the system secrecy diversity behavior, we perform the asymptotic SOP analysis in the high average channel gain regime. To explore further, we consider two scenarios: 1) Scenario I: when the quality of main channel is superior (i.e., $\Omega_{SD} \to \infty$), while Ω_{SE} is fixed. Such a scenario can be experienced when E is far away from S, whereas D is closer to S, and 2) Scenario II: when the quality of both the main channel and the wiretap channel are good (i.e., $\Omega_{SD} = \Omega_{SE} \to \infty$). Such a scenario may occur when both D and E are nearer to S.

1) SCENARIO I

Under this scenario, we perform an asymptotic SOP analysis for the case when $\Omega_{SD} \to \infty$ with fixed Ω_{SE}. For the given channel conditions, the asymptotic SOP expression can be presented as per the below theorem.

Theorem 2: The asymptotic SOP under Scenario I, $\tilde{\mathcal{P}}_{out}^{sec,I}(\eta)$, of the considered CRVN in the presence of nodes' mobility and imperfect channel estimates over Nakagami-m fading channels can be expressed as

$$\tilde{\mathcal{P}}_{out}^{sec,I}(\eta) = \zeta_1(\eta) + \zeta_2(\eta), \tag{21}$$

where $\zeta_1(\eta)$ and $\zeta_2(\eta)$ can be given, respectively, as

$$\begin{aligned}\zeta_1(\eta) = {} & 1 - \frac{1}{\Gamma(m_{SP})}\Upsilon\left(m_{SP}, \frac{m_{SP}}{\Omega_{SP}}c_1\right) - \sum_{a_1=0}^{N_D m_{SD}-1}\sum_{a_2=0}^{a_1} \\ & \times \sum_{a_3=0}^{N_E m_{SE}}\sum_{a_4=0}^{m_{SP}-1}\frac{1}{a_1!}\binom{N_E m_{SE}}{a_3}\binom{a_1}{a_2}\binom{m_{SP}-1}{a_4}\left(\frac{m_{SE}}{\Omega_{SE}}\right)^{-a_2} \\ & \times \left(\frac{m_{SP}}{\Omega_{SP}}\right)^{m_{SP}}\left(\frac{m_{SD}}{\alpha_{SD}}\right)^{a_3}(\eta-1)^{a_1-a_2}(\theta_2+c_1)^{N_E m_{SE}-a_3} \\ & \times \frac{\Gamma(N_E m_{SE}+a_2)\Gamma(a_3+a_4+1)}{\Gamma(N_E m_{SE})\Gamma(m_{SP})}\mathrm{e}^{-\left(\frac{m_{SP}c_1}{\Omega_{SP}}+\frac{m_{SD}(\eta-1)}{\alpha_{SD}}\right)} \\ & \times c_1^{m_{SP}-1-a_4}(\mathcal{B}+c_1)^{a_3+a_4-a_2-N_E m_{SE}+1}(\eta\varrho_1\alpha_2)^{a_4} \\ & \times \Psi\left(a_3+a_4+1, a_3+a_4-a_2-N_E m_{SE}+2, (\mathcal{B}+c_1)\frac{m_{SP}}{\Omega_{SP}}\right), \end{aligned} \tag{22}$$

$$\begin{aligned}\zeta_2(\eta) = {} & \frac{1}{\Gamma(m_{SP})}\Upsilon\left(m_{SP}, \frac{m_{SP}}{\Omega_{SP}}c_1\right) - \sum_{a_5=0}^{N_D m_{SD}-1}\sum_{a_6=0}^{a_5}\frac{1}{a_5!}\binom{a_5}{a_6} \\ & \times \frac{\Gamma(N_E m_{SE}+a_6)}{\Gamma(N_E m_{SE})\Gamma(m_{SP})}(\eta-1)^{a_5-a_6}\left(\frac{\eta\varrho_2\rho_{SE}^2}{\xi_2}\right)^{a_6}\mathrm{e}^{-\frac{m_{SD}(\eta-1)}{\alpha_{SD}}} \\ & \times \left(\frac{m_{SE}}{\Omega_{SE}}\right)^{N_E m_{SE}}\left(\frac{m_{SD}}{\alpha_{SD}}\right)^{a_5}\frac{\Upsilon\left(m_{SP}, \frac{m_{SP}}{\Omega_{SP}}c_1\right)}{\left(\frac{m_{SD}}{\alpha_{SD}}+\frac{\varrho_2\rho_{SE}^2\eta m_{SD}}{\alpha_{SD}\xi_2}\right)^{N_E m_{SE}+a_6}}, \end{aligned} \tag{23}$$

where $\alpha_{\mathrm{SD}} = \frac{\rho_{\mathrm{SD}}^2}{1-\rho_{\mathrm{SD}}^2}$ and $\mathcal{B} = \frac{\alpha_{\mathrm{SD}}\theta_2 m_{\mathrm{SE}} + \eta\varrho_1\alpha_2\Omega_{SE}m_{\mathrm{SD}}}{m_{\mathrm{SE}}\alpha_{\mathrm{SD}}}$.

Proof: See Appendix B for the detailed analysis. ■

Remark 3: From (21), we can see that the asymptotic SOP expression is independent of Ω_{SD}, and hence the SOP curves exhibit an irreducible error floor because of the presence of nodes' mobility and imperfect channel estimates. This results into a zero secrecy diversity order, as also demonstrated numerically in Section IV.

2) SCENARIO II

In this scenario, we present an asymptotic SOP analysis when $\Omega_{\mathrm{SD}}, \Omega_{\mathrm{SE}} \to \infty$ (i.e., the qualities of both the main and wiretap links are good), which can be evaluated according to the below theorem.

Theorem 3: The asymptotic SOP under Scenario II in the presence of nodes' mobility and imperfect channel estimates under Nakagami-*m* fading channels can be expressed as

$$\begin{aligned}\tilde{\mathcal{P}}_{\mathrm{out}}^{\mathrm{sec,II}}(\eta) &= 1 - \frac{m_{\mathrm{SE}}^{N_{\mathrm{E}}m_{\mathrm{SE}}}}{\Gamma(N_{\mathrm{E}}m_{\mathrm{SE}})}\sum_{b_1=0}^{N_{\mathrm{D}}m_{\mathrm{SD}}-1}\sum_{b_2=0}^{b_1}\frac{1}{b_1!}\binom{b_1}{b_2}\\ &\times(\eta-1)^{b_1-b_2}\left(\frac{m_{\mathrm{SD}}}{\alpha_{\mathrm{SD}}}\right)^{b_1}(\eta\alpha_{\mathrm{SE}})^{b_2}\mathrm{e}^{-\frac{(\eta-1)m_{\mathrm{SD}}}{\alpha_{\mathrm{SD}}}}\\ &\times\Gamma(N_{\mathrm{E}}m_{\mathrm{SE}}+b_2)\left(m_{\mathrm{SE}}+\frac{\eta\alpha_{\mathrm{SE}}m_{\mathrm{SD}}}{\alpha_{\mathrm{SD}}}\right)^{-(N_{\mathrm{E}}m_{\mathrm{SE}}+b_2)}. \quad (24)\end{aligned}$$

Proof: Please refer Appendix C for the derivation. ■

Remark 4: From (24), we can see that the asymptotic SOP expression is independent of both Ω_{SD} and Ω_{SE}. Thus, we can conclude that the system secrecy diversity order reduces to zero. This is because of two main reasons: 1) both the legitimate and the wiretap channels are able to simultaneously exploit the benefits of improved channel quality, and 2) the effects of imperfect channel estimates and nodes' mobility force the SOP curves to exhibit an irreducible error floor. This behavior is also reported in Section IV via numerical results.

C. PRACTICAL CASES OF INTEREST

In this section, we particularize the above reported findings to several practical cases of interest.

1) CASE 1: ALL MOBILE NODES WITH PERFECT CHANNEL ESTIMATES

When all nodes are mobile, we have $\rho_{S_J} \in [0, 1]$, for $J \in \{\mathrm{D}, \mathrm{E}, \mathrm{P}\}$. Also, we have $\Omega_{\epsilon_{S_J}} = 0$ for perfect channel estimates. We can have some key observations from this case.

- The exact SOP expression under this case can be obtained from (17) by substituting $\Omega_{w_{S_J}} = (1-\rho_{S_J}^2)\Omega_{e_{S_J}}$ and $\Omega_{e_{S_J}} = \Omega_{S_J}$, for $J \in \{\mathrm{D}, \mathrm{E}, \mathrm{P}\}$.
- The SOP asymptotic limit for the Scenario I ($\Omega_{\mathrm{SD}} \to \infty$ with fixed Ω_{SE}) under this case can be obtained from (21) by setting $\theta_2 = \frac{(1-\rho_{\mathrm{SP}}^2)\Omega_{\mathrm{SP}} + \varrho_1(1-\rho_{\mathrm{SE}}^2)\Omega_{\mathrm{SE}}}{\rho_{\mathrm{SP}}^2}$ and $c_1 = (\frac{\varrho_1}{\varrho_2} - (1-\rho_{\mathrm{SP}}^2)\Omega_{\mathrm{SP}})\frac{1}{\rho_{\mathrm{SP}}^2}$. Even in the case of perfect channel estimates, an irreducible secrecy error floor is also observed in the SOP curves, which is because of the presence of correlation parameters ρ_{SD}, ρ_{SE}, and ρ_{SP}, as also presented numerically in Section IV.
- The SOP asymptotic limit under Scenario II ($\Omega_{\mathrm{SD}} \to \infty$ and $\Omega_{\mathrm{SE}} \to \infty$) in (24) for this case remains unchanged, since the impact of imperfect channel estimates is negligible when Ω_{SD} and Ω_{SE} improve simultaneously. Hence, the SOP exhibits a saturation behavior due to the effects of nodes' mobility and simultaneous improvement in both the main and the wiretap channel qualities, as also shown in Section IV via numerical results.

2) CASE 2: ALL STATIC NODES WITH IMPERFECT CHANNEL ESTIMATES

Under this case, we have $\rho_{S_J} = 1$ (i.e., static nodes) and $\Omega_{\epsilon_{S_J}} \neq 0$ (i.e., imperfect channel estimates), for $J \in \{\mathrm{D}, \mathrm{E}, \mathrm{P}\}$. The following observations can be made from this case.

- Under this case, the exact SOP expression can be obtained by having the following modified parameters: $\Omega_{w_{S_J}} = \Omega_{\epsilon_{S_J}}$, $c_1 = (\frac{\varrho_1}{\varrho_2} - \Omega_{\epsilon_{\mathrm{SP}}})$, $\alpha_1 = 1$, $\alpha_2 = 1$, $\theta_1 = \Omega_{\epsilon_{\mathrm{SP}}} + \varrho_1\Omega_{\epsilon_{\mathrm{SD}}}$, $\theta_2 = \Omega_{\epsilon_{\mathrm{SP}}} + \varrho_1\Omega_{\epsilon_{\mathrm{SE}}}$, $\xi_1 = \varrho_2\Omega_{\epsilon_{\mathrm{SD}}} + 1$, and $\xi_2 = \varrho_2\Omega_{\epsilon_{\mathrm{SE}}} + 1$, in (17).
- The SOP asymptotic limit for the considered case can be obtained for the Scenario I ($\Omega_{\mathrm{SD}} \to \infty$ with fixed Ω_{SE}) from (21) by modifying the following parameters; $\alpha_{\mathrm{SD}} = 1$, $\theta_2 = \Omega_{\epsilon_{\mathrm{SP}}} + \varrho_1\Omega_{\epsilon_{\mathrm{SE}}}$, $\Omega_{w_{\mathrm{SE}}} = \Omega_{\epsilon_{\mathrm{SE}}}$, $\Omega_{w_{\mathrm{SP}}} = \Omega_{\epsilon_{\mathrm{SP}}}$, $c_1 = (\frac{\varrho_1}{\varrho_2} - \Omega_{\epsilon_{\mathrm{SP}}})$, $\alpha_2 = 1$, and $\rho_{\mathrm{SE}} = 1$. Consequently, it is observed that SOP curves attain an error floor in the high Ω_{SD}-regime, which also reduces the secrecy diversity order to zero. Such a behavior is also illustrated numerically in Section IV.
- The SOP asymptotic limit for the Scenario II ($\Omega_{\mathrm{SD}} \to \infty$ and $\Omega_{\mathrm{SE}} \to \infty$) under this case can be obtained from (24) by substituting $\alpha_{\mathrm{SD}} = \alpha_{\mathrm{SE}} = 1$. Consequently, $\tilde{\mathcal{P}}_{\mathrm{out}}^{\mathrm{sec,II}}(\eta)$ in (24) for this case can be expressed as

$$\begin{aligned}\tilde{\mathcal{P}}_{\mathrm{out}}^{\mathrm{sec,II}}(\eta) = 1 - \frac{m_{\mathrm{SE}}^{N_{\mathrm{E}}m_{\mathrm{SE}}}}{\Gamma(N_{\mathrm{E}}m_{\mathrm{SE}})}\sum_{b_1=0}^{N_{\mathrm{D}}m_{\mathrm{SD}}-1}\sum_{b_2=0}^{b_1}\frac{1}{b_1!}\binom{b_1}{b_2}\eta^{b_2}m_{\mathrm{SD}}^{b_1}\\ \times\frac{(\eta-1)^{b_1-b_2}}{(m_{\mathrm{SE}}+\eta m_{\mathrm{SD}})^{(N_{\mathrm{E}}m_{\mathrm{SE}}+b_2)}}\\ \times\mathrm{e}^{-(\eta-1)m_{\mathrm{SD}}}\Gamma(N_{\mathrm{E}}m_{\mathrm{SE}}+b_2). \quad (25)\end{aligned}$$

It is worth noting that (25) is independent of the parameters related to both the imperfect channel estimates and the nodes' mobility. However, the system still achieves a zero secrecy diversity order because of the simultaneous increase in both the legitimate and eavesdropper channel conditions, as shown numerically in Section IV.

3) CASE 3: ALL STATIC NODES WITH PERFECT CHANNEL ESTIMATES

Under this case, we have $\rho_{S_J} = 1$ (i.e., static nodes) and $\Omega_{\epsilon_{S_J}} = 0$ (i.e., perfect channel estimates), for $J \in \{\mathrm{D}, \mathrm{E}, \mathrm{P}\}$. Thus, we can re-express the instantaneous SNRs at terminals D and E as $\Lambda_{\mathrm{D}} = \min(\frac{\varrho_1}{\hat{X}}, \varrho_2)\hat{Y}$ and $\Lambda_{\mathrm{E}} = \min(\frac{\varrho_1}{\hat{X}}, \varrho_2)\hat{Z}$, respectively. Some key observations can be revealed from this case as

- By invoking the above SNRs obtained under this case into (14), and after some manipulations via [60, eq. (8.352.6)], [60, eq. (3.351.3)], and [60, eq. (3.351.2)], we can obtain $\mathcal{P}_{\mathrm{out}}^{\mathrm{sec}}(\eta)$ as (the detailed derivation is skipped for brevity)

$$\begin{aligned}
&\mathcal{P}_{\mathrm{out}}^{\mathrm{sec}}(\eta) \\
&= 1 - \sum_{a_1=0}^{N_{\mathrm{D}}m_{\mathrm{SD}}-1} \sum_{b_1=0}^{a_1} \frac{1}{a_1!}\binom{a_1}{b_1} \left(\frac{m_{\mathrm{SE}}}{\Omega_{\mathrm{SE}}}\right)^{N_{\mathrm{E}}m_{\mathrm{SE}}} \eta^{b_1} \\
&\times \left(\frac{m_{\mathrm{SP}}}{\Omega_{\mathrm{SP}}}\right)^{m_{\mathrm{SP}}} \left(\frac{m_{\mathrm{SD}}}{\Omega_{\mathrm{SD}}}\right)^{a_1} \frac{\Gamma(N_{\mathrm{E}}m_{\mathrm{SE}}+b_1)}{\Gamma(N_{\mathrm{E}}m_{\mathrm{SE}})\Gamma(m_{\mathrm{SP}})} \left(\frac{\eta-1}{\varrho_1}\right)^{a_1-b_1} \\
&\times \frac{\Gamma(a_1+m_{\mathrm{SP}}-b_1, \frac{(\eta-1)m_{\mathrm{SD}}}{\Omega_{\mathrm{SD}}\varrho_2} + \frac{m_{\mathrm{SP}}\varrho_1}{\Omega_{\mathrm{SP}}\varrho_2})}{\left(\frac{(\eta-1)m_{\mathrm{SD}}}{\Omega_{\mathrm{SD}}\varrho_1} + \frac{m_{\mathrm{SP}}}{\Omega_{\mathrm{SP}}}\right)^{a_1+m_{\mathrm{SP}}-b_1} \left(\frac{m_{\mathrm{SE}}}{\Omega_{\mathrm{SE}}} + \frac{m_{\mathrm{SD}}}{\Omega_{\mathrm{SD}}}\eta\right)^{N_{\mathrm{E}}m_{\mathrm{SE}}+b_1}} \\
&- \sum_{a_2=0}^{N_{\mathrm{D}}m_{\mathrm{SD}}-1} \sum_{b_2=0}^{a_2} \frac{1}{a_2!}\binom{a_2}{b_2} \left(\frac{m_{\mathrm{SE}}}{\Omega_{\mathrm{SE}}}\right)^{N_{\mathrm{E}}m_{\mathrm{SE}}} \left(\frac{m_{\mathrm{SD}}}{\Omega_{\mathrm{SD}}}\right)^{a_2} \\
&\times \frac{\Gamma(N_{\mathrm{E}}m_{\mathrm{SE}}+b_2)}{\Gamma(N_{\mathrm{E}}m_{\mathrm{SE}})\Gamma(m_{\mathrm{SP}})} \left(\frac{\eta-1}{\varrho_2}\right)^{a_2-b_2} \eta^{b_2} \mathrm{e}^{-\frac{(\eta-1)m_{\mathrm{SD}}}{\varrho_2\Omega_{\mathrm{SD}}}} \\
&\times \frac{1}{\left(\frac{m_{\mathrm{SE}}}{\Omega_{\mathrm{SE}}} + \frac{m_{\mathrm{SD}}\eta}{\Omega_{\mathrm{SD}}}\right)^{N_{\mathrm{E}}m_{\mathrm{SE}}+b_2}} \Upsilon\left(m_{\mathrm{SP}}, \frac{m_{\mathrm{SP}}\varrho_1}{\Omega_{\mathrm{SP}}\varrho_2}\right). \qquad (26)
\end{aligned}$$

- The SOP asymptotic limit in (26) for the scenario when $\Omega_{\mathrm{SD}} \to \infty$ with fixed Ω_{SE} can be expressed as

$$\begin{aligned}
&\tilde{\mathcal{P}}_{\mathrm{out}}^{\mathrm{sec}}(\eta) \\
&= \frac{\left(\frac{m_{\mathrm{SD}}}{\Omega_{\mathrm{SD}}}\right)^{N_{\mathrm{D}}m_{\mathrm{SD}}}}{\Gamma(N_{\mathrm{E}}m_{\mathrm{SE}})\Gamma(m_{\mathrm{SP}})(N_{\mathrm{D}}m_{\mathrm{SD}})!} \Bigg[\sum_{a_1=0}^{N_{\mathrm{D}}m_{\mathrm{SD}}} \binom{N_{\mathrm{D}}m_{\mathrm{SD}}}{a_1} \\
&\times \left(\frac{\eta-1}{\varrho_1}\right)^{N_{\mathrm{D}}m_{\mathrm{SD}}-a_1} \eta^{a_1} \Gamma(N_{\mathrm{E}}m_{\mathrm{SE}}+a_1) \left(\frac{m_{\mathrm{SE}}}{\Omega_{\mathrm{SE}}}\right)^{-a_1} \\
&\times \left(\frac{m_{\mathrm{SP}}}{\Omega_{\mathrm{SP}}}\right)^{-(N_{\mathrm{D}}m_{\mathrm{SD}}-a_1)} \Gamma\left(m_{\mathrm{SP}}+N_{\mathrm{D}}m_{\mathrm{SD}}-a_1, \frac{\varrho_1 m_{\mathrm{SP}}}{\varrho_2\Omega_{\mathrm{SP}}}\right) \\
&+ \sum_{a_2=0}^{N_{\mathrm{D}}m_{\mathrm{SD}}} \binom{N_{\mathrm{D}}m_{\mathrm{SD}}}{a_2} \left(\frac{\eta-1}{\varrho_2}\right)^{N_{\mathrm{D}}m_{\mathrm{SD}}-a_2} \eta^{a_2} \Gamma(N_{\mathrm{E}}m_{\mathrm{SE}}+a_2) \\
&\times \left(\frac{m_{\mathrm{SE}}}{\Omega_{\mathrm{SE}}}\right)^{-a_2} \Upsilon\left(m_{\mathrm{SP}}, \frac{m_{\mathrm{SP}}\varrho_1}{\Omega_{\mathrm{SP}}\varrho_2}\right) \Bigg]. \qquad (27)
\end{aligned}$$

From (27), we can infer that the considered system can achieve a full secrecy diversity order of $N_{\mathrm{D}}m_{\mathrm{SD}}$, under the case of static nodes and perfect channel estimates, as demonstrated numerically in Section IV.

- We can also obtain the SOP asymptotic limit in (26) for the scenario when $\Omega_{\mathrm{SD}} \to \infty$ and $\Omega_{\mathrm{SE}} \to \infty$ as

$$\begin{aligned}
\tilde{\mathcal{P}}_{\mathrm{out}}^{\mathrm{sec}}(\eta) &= 1 - \left(\frac{m_{\mathrm{SE}}}{\Omega_{\mathrm{SE}}}\right)^{N_{\mathrm{E}}m_{\mathrm{SE}}} \frac{\Gamma(N_{\mathrm{D}}m_{\mathrm{SD}}+N_{\mathrm{E}}m_{\mathrm{SE}})}{\Gamma(N_{\mathrm{E}}m_{\mathrm{SE}})} \\
&\times \sum_{b_1=0}^{N_{\mathrm{D}}m_{\mathrm{SD}}-1} \frac{1}{b_1!} \left(\frac{\eta m_{\mathrm{SD}}}{\Omega_{\mathrm{SD}}}\right)^{b_1} \\
&\times \left(\frac{m_{\mathrm{SE}}}{\Omega_{\mathrm{SE}}} + \frac{\eta m_{\mathrm{SD}}}{\Omega_{\mathrm{SD}}}\right)^{-N_{\mathrm{D}}m_{\mathrm{SD}}-N_{\mathrm{E}}m_{\mathrm{SE}}}. \qquad (28)
\end{aligned}$$

From (28), we can conclude that the system achieves a zero secrecy diversity order when $\Omega_{\mathrm{SD}}, \Omega_{\mathrm{SE}} \to \infty$, even though the nodes are static and channel estimation is perfect. This is due to the average channel strengths of both the main and wiretap links improve simultaneously.

D. IMPACT OF MAXIMUM TRANSMIT POWER $P_{\max}$ AND INTERFERENCE TEMPERATURE LIMIT $\mathcal{Q}$

In this section, we study the impact of maximum transmit power available at S, $P_{\max}$, and the interference temperature limit $\mathcal{Q}$, on the system's secrecy performance, which is illustrated in Corollaries 1 and 2.

Corollary 1: The SOP expression when $\mathcal{Q} = \kappa P_{\max}$, where κ is some positive constant and $P_{\max} \to \infty$, can be approximated as

$$\begin{aligned}
\mathcal{P}_{\mathrm{out}}^{\mathrm{sec,C1}}(\eta) &\approx 1 - \frac{1}{\Gamma(N_{\mathrm{E}}m_{\mathrm{SE}})} \left(\frac{m_{\mathrm{SE}}}{\Omega_{\mathrm{SE}}}\right)^{N_{\mathrm{E}}m_{\mathrm{SE}}} \mathrm{e}^{-\frac{(\eta-1)m_{\mathrm{SD}}\Omega_{w_{\mathrm{SD}}}}{\rho_{\mathrm{SD}}^2\Omega_{\mathrm{SD}}}} \\
&\times \sum_{p_1=0}^{N_{\mathrm{D}}m_{\mathrm{SD}}-1} \sum_{p_2=0}^{p_1} \frac{1}{p_1!}\binom{p_1}{p_2} (\eta-1)^{p_1-p_2} \\
&\times \left(\frac{\rho_{\mathrm{SE}}^2}{\Omega_{w_{\mathrm{SE}}}}\right)^{p_2} \left(\frac{\Omega_{w_{\mathrm{SD}}}}{\rho_{\mathrm{SD}}^2}\right)^{p_1} \\
&\times \left(\frac{m_{\mathrm{SD}}}{\Omega_{\mathrm{SD}}}\right)^{p_1} \frac{\Gamma(p_2+N_{\mathrm{E}}m_{\mathrm{SE}})}{\left(\frac{\rho_{\mathrm{SE}}^2\Omega_{w_{\mathrm{SD}}}m_{\mathrm{SD}}}{\rho_{\mathrm{SD}}^2\Omega_{\mathrm{SD}}\Omega_{w_{\mathrm{SE}}}} + \frac{m_{\mathrm{SE}}}{\Omega_{\mathrm{SE}}}\right)^{p_2+N_{\mathrm{E}}m_{\mathrm{SE}}}}. \qquad (29)
\end{aligned}$$

Proof: The proof is given in Appendix D. ■

Remark 5: The approximate SOP expression in (29) is independent of $P_{\max}$, however, it is affected by the nodes' mobility and imperfect channel estimates. Therefore, the achievable secrecy diversity order of the considered system is zero.

Remark 6: The SOP in (29) is also independent of average channel gain of S → P link, i.e., Ω_{SP}, as with $\mathcal{Q}$ being proportional to $P_{\max}$, the secondary system performance is no longer limited by the primary receiver interference constraint.

Corollary 2: For the case when $\mathcal{Q} \neq \kappa P_{\max}$. At high value of $P_{\max}$, i.e., $P_{\max} \to \infty$, the SOP can be expressed as

$$\mathcal{P}_{\text{out}}^{\text{sec,C2}}(\eta) \approx 1 - \Delta \times \Psi\Bigg(u_2+m_{\text{SP}}+u_4, u_2+m_{\text{SP}}+u_4-N_{\text{E}}m_{\text{SE}} - u_1 + 1, \frac{\beta_2}{\beta_1}\left(\frac{m_{\text{SD}}(\eta-1)}{\Omega_{\text{SD}}\varrho_1\alpha_1}+\frac{m_{\text{SP}}}{\Omega_{\text{SP}}}\right)\Bigg), \quad (30)$$

where

$$\Delta = \frac{1}{\Gamma(N_{\text{E}}m_{\text{SE}})\Gamma(m_{\text{SP}})}\left(\frac{m_{\text{SE}}}{\Omega_{\text{SE}}}\right)^{N_{\text{E}}m_{\text{SE}}}\left(\frac{m_{\text{SP}}}{\Omega_{\text{SP}}}\right)^{m_{\text{SP}}} \times \sum_{u=0}^{N_{\text{D}}m_{\text{SD}}-1}\frac{1}{u!}\left(\frac{m_{\text{SD}}}{\Omega_{\text{SD}}}\right)^{u}\sum_{u_1=0}^{u}\binom{u}{u_1}\sum_{u_2=0}^{u}\binom{u}{u_2}\sum_{u_4=0}^{N_{\text{E}}m_{\text{SE}}} \times \binom{N_{\text{E}}m_{\text{SE}}}{u_4}(\eta\alpha_2)^{u_1}\alpha_1^{N_{\text{E}}m_{\text{SE}}+u_1-u}\theta_2^{N_{\text{E}}m_{\text{SE}}-u_4}\theta_1^{u-u_2} \times \Gamma(N_{\text{E}}m_{\text{SE}}+u_1)\left(\frac{\Omega_{\text{SD}}\Omega_{\text{SE}}}{\beta_1}\right)^{N_{\text{E}}m_{\text{SE}}+u_1}\Gamma(u_2+m_{\text{SP}}+u_4) \times \mathrm{e}^{-\left(\frac{m_{\text{SD}}(\eta-1)\theta_1}{\Omega_{\text{SD}}\varrho_1\alpha_1}\right)}\left(\frac{\beta_2}{\beta_1}\right)^{u_2+m_{\text{SP}}+u_4-N_{\text{E}}m_{\text{SE}}-u_1}\left(\frac{\eta-1}{\varrho_1}\right)^{u-u_1}. \quad (31)$$

Proof: The proof is presented in Appendix E. ■

Remark 7: Corollary 2 shows that the approximated SOP under the case when S has excessive transmit power (i.e., $P_{\max} \to \infty$) is independent of $P_{\max}$, and the SOP performance is dictated by the interference temperature limit $\mathcal{Q}$. Therefore, the system achieves a zero secrecy diversity order. This indicates that although the source has unlimited power to transmit, but the interference temperature constraint limits the advantage of excessive transmit power (as $P_{\text{S}} = \frac{\mathcal{Q}}{\rho_{\text{SP}}^2|\hat{h}_{\text{SP}}|^2+\Omega_{w_{\text{SP}}}}$) alongwith the impact of nodes' mobility and imperfect channel estimates.

E. ESC ANALYSIS

The ESC represents the rate below which an average secure communication is possible. We can define ESC as

$$\overline{\mathbb{C}}_{\text{sec}} = \frac{1}{\ln(2)}\mathbb{E}\left[\mathbb{C}_s(\Lambda_{\text{D}}, \Lambda_{\text{E}})\right], \quad (32)$$

where $\mathbb{C}_{\text{sec}}(\Lambda_{\text{D}}, \Lambda_{\text{E}}) = \max[\ln(1+\Lambda_{\text{D}}) - \ln(1+\Lambda_{\text{E}}), 0]$ is the instantaneous secrecy channel capacity. Now, by the use of (12) and (13), we can express $\overline{\mathbb{C}}_{\text{sec}}$ as

$$\overline{\mathbb{C}}_{\text{sec}} = \frac{1}{\ln(2)}\underbrace{\mathbb{E}\left[\ln\left(1+\frac{\varrho_1\alpha_1\hat{Y}}{\hat{X}+\theta_1}\right)-\ln\left(1+\frac{\varrho_1\alpha_2\hat{Z}}{\hat{X}+\theta_2}\right)\middle|\hat{X} > c_1\right]}_{\triangleq\overline{\mathbb{C}}_{\text{sec},1}} + \frac{1}{\ln(2)}\underbrace{\mathbb{E}\left[\ln\left(1+\frac{\hat{Y}}{\tilde{\xi}_1}\right)-\ln\left(1+\frac{\hat{Z}}{\tilde{\xi}_2}\right)\middle|\hat{X} < c_1\right]}_{\triangleq\overline{\mathbb{C}}_{\text{sec},2}}, \quad (33)$$

where $\tilde{\xi}_1 = \frac{\xi_1}{\varrho_2\rho_{\text{SD}}^2}$, $\tilde{\xi}_2 = \frac{\xi_2}{\varrho_2\rho_{\text{SE}}^2}$. Further, we evaluate the analytical expression for the ESC as per the following theorem.

Theorem 4: The ESC, $\overline{\mathbb{C}}_{\text{sec}}$, of the considered CRVN in the presence of nodes' mobility and imperfect channel estimates over Nakagami-m fading channels can be expressed as

$$\overline{\mathbb{C}}_{\text{sec}} = \frac{1}{\ln(2)}\left[\overline{\mathbb{C}}_{\text{sec},1} + \overline{\mathbb{C}}_{\text{sec},2}\right], \quad (34)$$

where $\overline{\mathbb{C}}_{\text{sec},1}$ and $\overline{\mathbb{C}}_{\text{sec},2}$ are given in (35) and (36), respectively, as shown at the bottom of the next page, with $\tau_1 = \frac{m_{\text{SD}}}{\Omega_{\text{SD}}\varrho_1\alpha_1}$, $\tau_2 = \frac{1}{\varrho_1\alpha_1}(\frac{m_{\text{SD}}}{\Omega_{\text{SD}}} + \frac{m_{\text{SE}}}{\Omega_{\text{SE}}})$, $\tilde{\tau}_1 = \frac{\alpha_1\tau_1}{\alpha_2}$, $\tilde{\tau}_2 = \frac{\alpha_1\tau_2}{\alpha_2}$, and $w_i = \frac{x_i}{((\mathbb{U}+1)L_{\mathbb{U}+1}(x_i))^2}$ and x_i, $(i = 1, \ldots, \mathbb{U})$ are weights and zeros of $\mathbb{U}$-order Gauss-Laguerre polynomial (i.e., $L_{\mathbb{U}}(t)$) [65].

Proof: See Appendix F for the detailed derivation. ■

Remark 8: From (34), we can see that $\overline{\mathbb{C}}_{\text{sec}}$ comprises of finite summations, complete gamma functions, lower incomplete gamma functions, exponentials, and the Meijer-$\mathcal{G}$ functions. The functions depend on various system/channel parameters, such as, number of antennas ($N_{\text{D}}, N_{\text{E}}$), fading severity parameters ($m_{\text{SD}}, m_{\text{SE}}, m_{\text{SP}}$), channel estimation errors ($\Omega_{\epsilon_{\text{SD}}}, \Omega_{\epsilon_{\text{SE}}}, \Omega_{\epsilon_{\text{SP}}}$), time varying errors ($\Omega_{e_{\text{SD}}}, \Omega_{e_{\text{SE}}}, \Omega_{e_{\text{SP}}}$), correlation coefficients ($\rho_{\text{SD}}, \rho_{\text{SE}}, \rho_{\text{SP}}$), and average transmit SNRs (ϱ_1, ϱ_2). Therefore, the ESC expression can be numerically evaluated for different involved system/channel parameters using the Mathematica computational software package.

IV. NUMERICAL RESULTS AND DISCUSSIONS

This section presents the numerical results (via Mathematica) and Monte-Carlo simulations averaged for 10^6 independent trials (using Matlab) to verify the correctness of our derived analytical results. It is to be noted that the correlation parameter $\rho_{\iota\jmath} = J_0(\frac{2\pi f_c v_{\iota\jmath}}{Rc})$ is a function of relative velocity $v_{\iota\jmath}$, for $\iota\jmath \in \{\text{SD}, \text{SE}, \text{SP}\}$, and both follow inverse relationship. Specifically, $\rho_{\iota\jmath} \to 0$ (i.e., severe time-selective fading) corresponds to extremely high mobility scenario, and $\rho_{\iota\jmath} = 1$ corresponds to non-moving (i.e.,$v_{\iota\jmath} = 0$) scenario and channel experiences quasi-static behavior. In addition, we plot the curves for fixed values of velocities (in Figs. 2–4, Figs. 6–9, and Fig. 11) as well as for varying velocities (in Fig. 5 and Fig. 10). Furthermore, we plot the curves for various values of average channel variances,[2] i.e., Ω_{SD}, Ω_{SE}, and Ω_{SP}. For numerical investigations, we set $\mathbb{U} = 9$ as the Gauss-Laguerre polynomial order to accurately evaluate the ESC results[3], $N_0 = 0$ dB, code rate $R = 9.6$ kbps, speed of light $c = 3 \times 10^8$ m/s, carrier frequency $f_c = 1.9 \times 10^9$ Hz.

[2]It is to be noted that the auto-regression process can also be simulated by applying the path-loss modeling, such that $\Omega_{\iota\jmath}(k) = d_{\iota\jmath}^{-\nu}(k)$ at kth signaling instant, where ν is the path-loss exponent, $d_{\iota\jmath}(k) = d_0 + kv_{\iota\jmath}(k)$, d_0 denotes the reference distance, and $v_{\iota\jmath}$ is the relative velocity between the nodes ι and $\jmath$ [66].

[3]Note that Table 1 (shown at the top of the next page) demonstrates that the difference between the exact ESC analysis and the approximate ESC analysis using Gauss-Laguerre method is very small for a broad range of ϱ_1 (dB), under various set of channel/system parameters.

TABLE I Difference Between Exact ESC and Approximate ESC Expressions (With $\Omega_{SD} = 10$ dB, $\Omega_{SE} = \Omega_{SP} = 0$ dB, $\varrho_2 = 30$ dB, and $v_{SD} = v_{SE} = v_{SP} = 50$ km/h)

	ϱ_1(dB)	0	5	10	15	20	25	30	35	40
$\Omega_e = 0.01$, $\Omega_\epsilon = 0.1$, $(m_{SD}, N_D) = (1,1)$, $(m_{SE}, N_E) = (1,1)$, $m_{SP} = 1$	Exact Analysis	2.2062	2.6203	2.8907	3.05955	3.0498	3.0670	3.0852	3.0802	3.0820
$\Omega_e = 0.01$, $\Omega_\epsilon = 0.1$, $(m_{SD}, N_D) = (1,1)$, $(m_{SE}, N_E) = (1,1)$, $m_{SP} = 1$	Guass-Laguerre with $\mathbb{U} = 3$	2.10578	2.59574	2.87793	3.00906	3.06022	3.07778	3.083	3.08396	3.084
$\Omega_e = 0.01$, $\Omega_\epsilon = 0.1$, $(m_{SD}, N_D) = (1,1)$, $(m_{SE}, N_E) = (1,1)$, $m_{SP} = 1$	Guass-Laguerre with $\mathbb{U} = 7$	2.12497	2.59944	2.87821	3.00907	3.06022	3.07778	3.083	3.08396	3.084
$\Omega_e = 0.01$, $\Omega_\epsilon = 0.1$, $(m_{SD}, N_D) = (1,1)$, $(m_{SE}, N_E) = (1,1)$, $m_{SP} = 1$	Guass-Laguerre with $\mathbb{U} = 9$	2.17624	2.61956	2.88822	3.00907	3.06022	3.07778	3.083	3.08396	3.084
$\Omega_e = 0.1$, $\Omega_\epsilon = 0.1$, $(m_{SD}, N_D) = (3,2)$, $(m_{SE}, N_E) = (2,1)$, $m_{SP} = 1$	Exact Analysis	3.3718	3.9051	4.1771	4.2944	4.3353	4.3553	4.3617	4.3527	4.3684
$\Omega_e = 0.1$, $\Omega_\epsilon = 0.1$, $(m_{SD}, N_D) = (3,2)$, $(m_{SE}, N_E) = (2,1)$, $m_{SP} = 1$	Guass-Laguerre with $\mathbb{U} = 3$	3.32011	3.87116	4.17177	4.29907	4.33052	4.35554	4.35964	4.36039	4.36042
$\Omega_e = 0.1$, $\Omega_\epsilon = 0.1$, $(m_{SD}, N_D) = (3,2)$, $(m_{SE}, N_E) = (2,1)$, $m_{SP} = 1$	Guass-Laguerre with $\mathbb{U} = 7$	3.35741	3.90161	4.17484	4.29907	4.33152	4.35554	4.35964	4.36039	4.36042
$\Omega_e = 0.1$, $\Omega_\epsilon = 0.1$, $(m_{SD}, N_D) = (3,2)$, $(m_{SE}, N_E) = (2,1)$, $m_{SP} = 1$	Guass-Laguerre with $\mathbb{U} = 9$	3.37178	3.90363	4.17584	4.29907	4.33152	4.35554	4.35964	4.36039	4.36042

A. SECRECY OUTAGE PROBABILITY

1) IMPACT OF FADING SEVERITY AND MULTIPLE ANTENNAS ON SOP

In Fig. 2, we illustrate the effects of fading severity parameters associated with the main and wiretap channels (i.e., m_{SD} and m_{SE}) and the number of antennas (i.e., N_D and N_E) on the SOP performance, when $\mathcal{R}_s = 0.1$ bps/Hz, $\varrho_1 = 10$ dB, $\varrho_2 = 20$ dB, $\Omega_{SE} = 10$ dB, $\Omega_{SP} = 0$ dB, and $m_{SP} = 1$. Also, the time varying error can be evaluated with the help of the relation $\Omega_{e_{S_J}} = \Omega_{\epsilon_{S_J}} + \Omega_{S_J}$, for $J \in \{D, E, P\}$. In particular, Fig. 2(a) considers the impact of both nodes' mobility ($v_{S_J} = 50$ km/h) and imperfect channel estimates ($\Omega_{\epsilon_{S_J}} = 0.01$), while Fig. 2(b) considers the scenario with static nodes ($v_{S_J} = 0$ km/h) and perfect channel estimates ($\Omega_{\epsilon_{S_J}} = 0$), for $J \in \{D, E, P\}$. From the plots in Fig. 2(a), we can see that the derived SOP results in (17) match perfectly with the simulation results over the entire regime of Ω_{SD}. Furthermore, the asymptotic SOP results in (21) are in good agreement with the exact results in the medium-to-high SNR regime. This corroborates the accuracy of our derived findings. Also, we can observe from Fig. 2(a) that the SOP performance first improves with an increase in Ω_{SD} in the low-to-medium Ω_{SD} regime, and then exhibits a saturation floor in the high SNR regime, irrespective of m_{SD}, m_{SE}, N_D, and N_E. The SOP performance enhancement in low-to-medium Ω_{SD} regime is due to the improved quality of the legitimate S $\rightarrow$ D link, however, this benefit is overshadowed by the effects of nodes' mobility and imperfect channel estimates in the high SNR regime and results into the irreducible error floor. This saturation in the SOP curves further implies that the system's secrecy diversity order reduces to zero, as also analytically demonstrated in Section III-B under Scenario I. Moreover,

$$\overline{\mathbb{C}}_{\text{sec},1} = \left(\frac{m_{SP}}{\Omega_{SP}}\right)^{m_{SP}} \frac{e^{-\frac{m_{SP}}{\Omega_{SP}}c_1}}{\Gamma(m_{SP})\Gamma(N_D m_{SD})} \sum_{n_3=0}^{m_{SP}-1} \binom{m_{SP}-1}{n_3} c_1^{m_{SP}-1-n_3} \sum_{i=0}^{\mathbb{U}} w_i x_i^{n_3} \Bigg\{ \left(\frac{1}{\tau_1}\right)^{n_3+1} e^{-\left(\frac{m_{SP}}{\Omega_{SP}\tau_1}-1\right)x_i}$$
$$\times \mathcal{G}_{2,3}^{3,1}\left(x_i + (\theta_1 + c_1)\tau_1 \Big|_{N_D m_{SD},0,0}^{0,1}\right) - \sum_{n_1=0}^{N_E m_{SE}-1} \frac{1}{n_1!}\left(\frac{m_{SE}}{\Omega_{SE}}\right)^{n_1}\left(\frac{m_{SD}}{\Omega_{SD}} + \frac{m_{SE}}{\Omega_{SE}}\right)^{-N_D m_{SD}-n_1} e^{-\left(\frac{m_{SP}}{\Omega_{SP}\tau_2}-1\right)x_i}$$
$$\times \left(\frac{1}{\tau_2}\right)^{n_3+1} \mathcal{G}_{2,3}^{3,1}\left(x_i + (\theta_1 + c_1)\tau_2 \Big|_{N_D m_{SD}+n_1,0,0}^{0,1}\right) - \frac{\Gamma(N_D m_{SD})}{\Gamma(N_E m_{SE})} \sum_{n_2=0}^{N_D m_{SD}-1} \frac{1}{n_2!}\left(\frac{m_{SD}}{\Omega_{SD}}\right)^{n_2} e^{-\left(\frac{m_{SP}}{\Omega_{SP}\bar{\tau}_2}-1\right)x_i}$$
$$\times \left(\frac{m_{SD}}{\Omega_{SD}} + \frac{m_{SE}}{\Omega_{SE}}\right)^{-N_E m_{SE}-n_2} \left(\frac{1}{\tilde{\tau}_2}\right)^{n_3+1} \mathcal{G}_{2,3}^{3,1}\left(x_i + (\theta_2 + c_1)\tilde{\tau}_2 \Big|_{N_E m_{SE}+n_2,0,0}^{0,1}\right) \Bigg\}, \tag{35}$$

$$\overline{\mathbb{C}}_{\text{sec},2} = \Bigg\{ \frac{1}{\Gamma(N_D m_{SD})} \mathcal{G}_{3,2}^{1,3}\left(\frac{\Omega_{SD}}{m_{SD}\tilde{\xi}_1} \Big|_{1,0}^{1-N_D m_{SD},1,1}\right) - \frac{1}{\Gamma(N_D m_{SD})} \sum_{n_4=0}^{N_E m_{SE}-1} \frac{1}{n_4!}\left(\frac{m_{SE}}{\Omega_{SE}}\right)^{n_4}\left(\frac{m_{SD}}{\Omega_{SD}}\right)^{N_D m_{SD}}$$
$$\times \left(\frac{m_{SD}}{\Omega_{SD}} + \frac{m_{SE}}{\Omega_{SE}}\right)^{-N_D m_{SD}-n_4} \mathcal{G}_{3,2}^{1,3}\left(\frac{1}{\tilde{\xi}_1\left(\frac{m_{SD}}{\Omega_{SD}} + \frac{m_{SE}}{\Omega_{SE}}\right)} \Big|_{1,0}^{1-N_D m_{SD}-n_4,1,1}\right) - \frac{1}{\Gamma(N_E m_{SE})} \sum_{n_5=0}^{N_D m_{SD}-1} \frac{1}{n_5!}\left(\frac{m_{SD}}{\Omega_{SD}}\right)^{n_5}$$
$$\times \left(\frac{m_{SE}}{\Omega_{SE}}\right)^{N_E m_{SE}} \left(\frac{m_{SD}}{\Omega_{SD}} + \frac{m_{SE}}{\Omega_{SE}}\right)^{-N_E m_{SE}-n_5} \mathcal{G}_{3,2}^{1,3}\left(\frac{1}{\tilde{\xi}_2\left(\frac{m_{SD}}{\Omega_{SD}} + \frac{m_{SE}}{\Omega_{SE}}\right)} \Big|_{1,0}^{1-N_E m_{SE}-n_5,1,1}\right) \Bigg\} \frac{\Upsilon(m_{SP}, \frac{m_{SP}}{\Omega_{SP}}c_1)}{\Gamma(m_{SP})}, \tag{36}$$

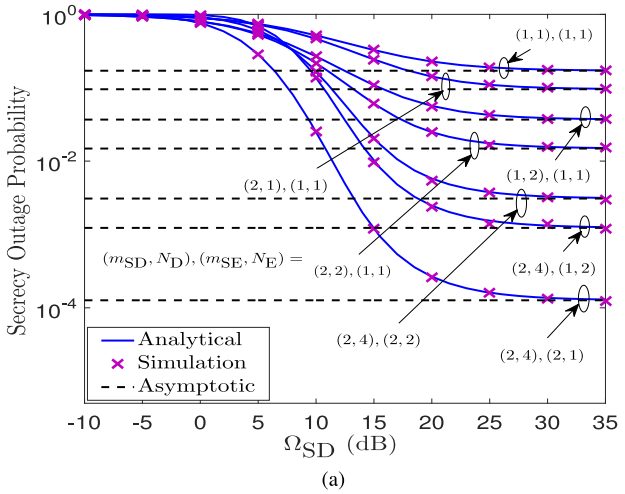

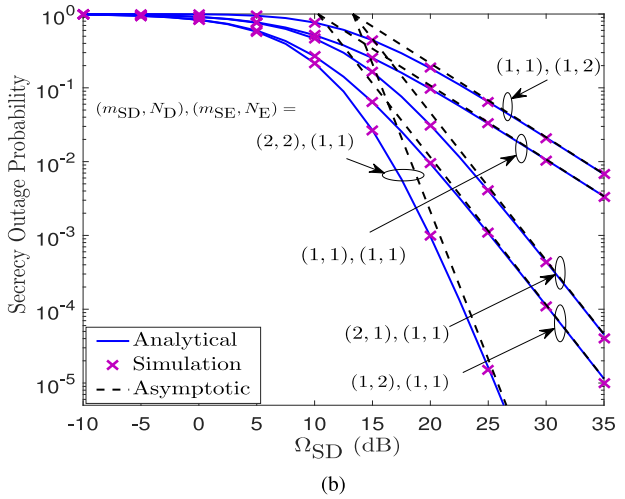

FIGURE 2. SOP versus Ω_{SD} for different values of secondary channels fading severity, N_{D}, and N_{E} (a) with nodes' mobility and imperfect channel estimates, and (b) with static nodes and perfect channel estimates.

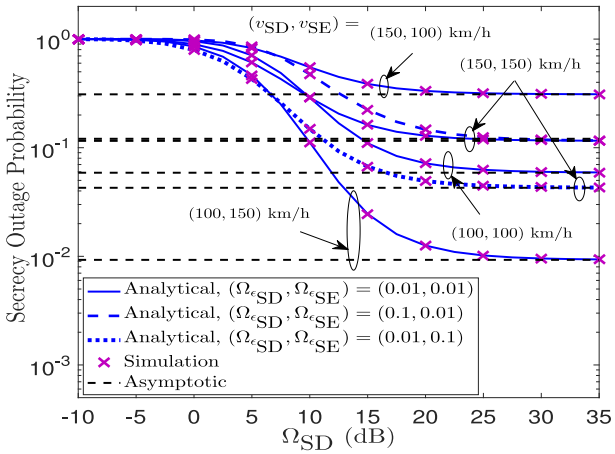

FIGURE 3. SOP versus Ω_{SD} for different v_{SD} and v_{SE}.

from Fig. 2(b), we can infer that our derived theoretical results are in perfect agreement with the simulation studies, and hence verifying the accuracy of our analytical findings. On the contrary to Fig. 2(a), the plots in Fig. 2(b) exhibit a significant improvement in the SOP performance over the entire range of Ω_{SD}. The secrecy diversity order of $N_{\mathrm{D}}m_{\mathrm{SD}}$ can also be verified from the curves for various values of N_{D} and m_{SD}. This is because of the absence of combined impact of nodes' mobility and imperfect channel estimates, as presented via analytical findings in Section III-C.

Furthermore, it can be observed from Fig. 2(a) and (b) that the SOP performance increases significantly with the increased fading severity parameter of main channel m_{SD} and/or number of antennas at the destination N_{D}, since the higher values of m_{SD} and/or N_{D} strengthen the quality of legitimated link. As expected, higher values of m_{SE} and/or N_{E} enhance the wiretap channel quality and hence increase the probability of successful eavesdropping, which results into the SOP performance degradation. In addition, we can infer from Fig. 2(a) and Fig. 2(b) that the impact of number of antennas (N_{D} and N_{E}) on the SOP performance is more prominent than that of fading severity parameters (m_{SD} and m_{SE}).

2) IMPACT OF NODES' MOBILITY, TIME VARYING ERRORS, AND IMPERFECT CHANNEL ESTIMATES ON SOP

Fig. 3 illustrates the SOP as a function of Ω_{SD} for various combinations of v_{SD}, v_{SE}, $\Omega_{\epsilon_{\mathrm{SD}}}$, and $\Omega_{\epsilon_{\mathrm{SE}}}$, when $\mathcal{R}_s = 0.1$ bps/Hz, $\varrho_1 = 10$ dB, $\varrho_2 = 20$ dB, $\Omega_{\mathrm{SE}} = 10$ dB, $\Omega_{\mathrm{SP}} = 0$ dB, $m_{\mathrm{SP}} = 1$, $(m_{\mathrm{SD}}, N_{\mathrm{D}}) = (2, 3)$, $(m_{\mathrm{SE}}, N_{\mathrm{E}}) = (2, 2)$, $v_{\mathrm{SP}} = 20$ km/h, and $\Omega_{\epsilon_{\mathrm{SP}}} = 0.01$. We also set $\Omega_{e_{\mathrm{S}_J}} = \Omega_{\epsilon_{\mathrm{S}_J}} + \Omega_{\mathrm{S}_J}$, for $J \in \{\mathrm{D}, \mathrm{E}, \mathrm{P}\}$. From the plots in Fig. 3, it can be observed that the SOP decreases as relative velocity between vehicles S and D, v_{SD}, and between vehicles S and E, v_{SE}, increase, i.e., for high speed scenario. This is due to the reason that higher values of relative velocity increase the likelihood of the channel to undergo time-selective fading. By following the above reasoning, we can further justify the trends observed from the plots in Fig. 3, where the SOP performance degrades more severely for the case when $v_{\mathrm{SD}} > v_{\mathrm{SE}}$ and improves significantly for the case when $v_{\mathrm{SD}} < v_{\mathrm{SE}}$. Moreover, it can also be seen from this figure that as $\Omega_{\epsilon_{\mathrm{SD}}}$ increases (i.e., from $\Omega_{\epsilon_{\mathrm{SD}}} = 0.01$ to $\Omega_{\epsilon_{\mathrm{SD}}} = 0.1$), the SOP performance deteriorates, whereas the SOP performance improves as $\Omega_{\epsilon_{\mathrm{SE}}}$ increases from 0.01 to 0.1. This implies that it is always favorable to have poorer estimation conditions for wiretap channel and better channel estimates for main channel. Also, the joint impact of nodes' mobility and imperfect channel estimates reduces the secrecy diversity order to zero.

In Fig. 4, we investigate the SOP performance for the considered system versus γ (with $\gamma = \varrho_1 = \varrho_2$) for various values of Ω_ϵ (where $\Omega_\epsilon = \Omega_{\epsilon_{\mathrm{SD}}} = \Omega_{\epsilon_{\mathrm{SE}}} = \Omega_{\epsilon_{\mathrm{SP}}}$), N_{D}, and N_{E}, when $\mathcal{R}_s = 0.1$ bps/Hz, $\Omega_{\mathrm{SD}} = 5$ dB, $\Omega_{\mathrm{SE}} = 0$ dB, $\Omega_{\mathrm{SP}} = 0$ dB, $m_{\mathrm{SP}} = 1$, $m_{\mathrm{SD}} = 2$, $m_{\mathrm{SE}} = 1$, $v_{\mathrm{S}_J} = 50$ km/h, and $\Omega_{e_{\mathrm{S}_J}} = 0.01$, for $J \in \{\mathrm{D}, \mathrm{E}, \mathrm{P}\}$. From Fig. 4, we can see that the approximate SOP expression derived in (29) under the case of

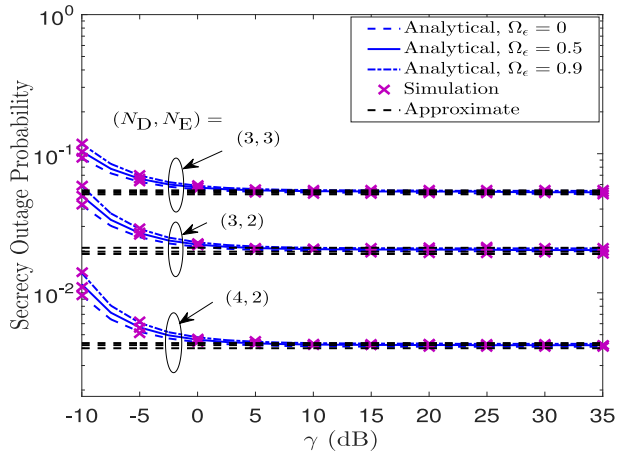

FIGURE 4. SOP versus γ for different Ω_ϵ, N_D, and N_E.

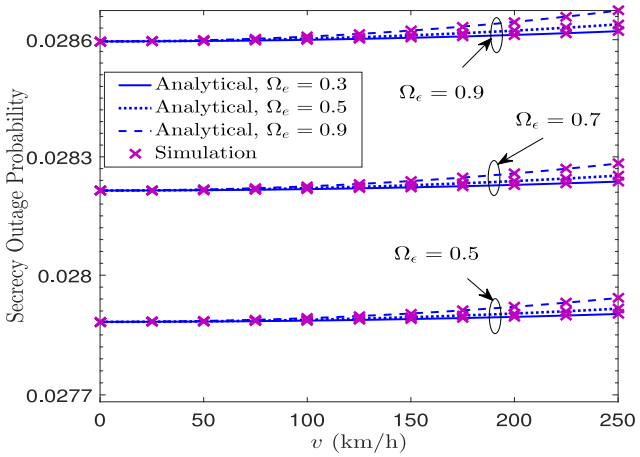

FIGURE 5. OP versus v for different Ω_e and Ω_ϵ.

$P_{\max} \to \infty$ completely agrees with the exact SOP analytical analysis derived in (17), and hence validates the accuracy of our proposed analysis. Moreover, we can observe that the system's SOP performance first improves in the low γ regime and then achieves an irreducible secrecy floor, irrespective of the other involved parameters. This behavior occurs due to the simultaneous strengthening of both the main and wiretap channels along with the detrimental effects of nodes' mobility and imperfect channel estimates. From this behavior, one can observe that the secrecy diversity order reduces to zero. Furthermore, for a fixed N_D and N_E, as the error in the channel estimation increases, the SOP performance degrades. As expected, it can also be seen from this figure that the SOP performance improves as N_D increases, while it decreases as N_E increase.

In Fig. 5, we illustrate the SOP performance as a function of relative velocity ($v = v_{S_J}$ km/h), for different values of time varying errors ($\Omega_e = \Omega_{e_{S_J}}$) and channel estimation errors ($\Omega_\epsilon = \Omega_{\epsilon_{S_J}}$), for $J \in \{D, E, P\}$, when $\mathcal{R}_s = 0.1$ bps/Hz, $\Omega_{SD} = 10$ dB, $\Omega_{SE} = 5$ dB, $\Omega_{SP} = 0$ dB, $m_{SP} = 1$, $(m_{SD}, N_D) = (2, 2)$, $(m_{SE}, N_E) = (1, 1)$, $\varrho_1 = 0$ dB, $\varrho_2 =$

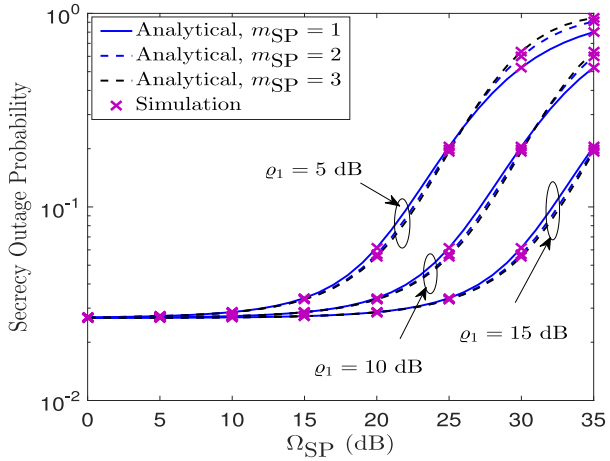

FIGURE 6. Impact of Ω_{SP} on the SOP performance for various ϱ_1 and m_{SP}.

30 dB. From the plots, it is evident that as v increases, the system's SOP performance decreases for the considered velocity ranges. This is because of the reason that an increase in the velocity increases the likelihood of all the associated channels (i.e., legitimated, wiretap, and interference) to undergo the time-selective fading. We can also infer that as Ω_e and/or Ω_ϵ increase, the system's SOP performance further degrades. Thus, we can conclude that the nodes' mobility, time-varying errors, and imperfect channel estimates have a severe impact on the system's SOP performance.

3) IMPACT OF PRIMARY RECEIVER ON SOP

Fig. 6 plots the SOP as a function of interference channel condition Ω_{SP} for different values of fading severity parameter m_{SP} of the interference channel, and the interference temperature limit ϱ_1 (where $\varrho_1 = \frac{Q}{N_0}$), when $\mathcal{R}_s = 0.1$ bps/Hz, $\Omega_{SD} = 10$ dB, $\Omega_{SE} = 5$ dB, $(m_{SD}, N_D) = (2, 2)$, $(m_{SE}, N_E) = (1, 1)$, $\varrho_2 = 30$ dB, $v_{S_J} = 50$ km/h $\Omega_{\epsilon_{S_J}} = 0.1$, and $\Omega_{e_{S_J}} = 0.01$, $J \in \{D, E, P\}$. From the plots in Fig. 6, we can see that as the interference channel quality Ω_{SP} increases (i.e., the interference imposed by the secondary network transmissions to the primary receiver increases), the SOP performance degrades significantly. This is owing to the reason that the transmit power at secondary source decreases as Ω_{SP} increases. Furthermore, the SOP performance improves as ϱ_1 increases, which is due to the fact that an increase in ϱ_1 allows the secondary system to transmit at a higher power level without interfering the primary receiver. Also, it can be observed that an increase in the value of fading severity parameter for the interference channel have a very minimal impact on the SOP performance. Thus, from Fig. 6, we can conclude that Ω_{SP} significantly affects the SOP performance, whereas, the SOP performance is almost unaffected with an increase in m_{SP}.

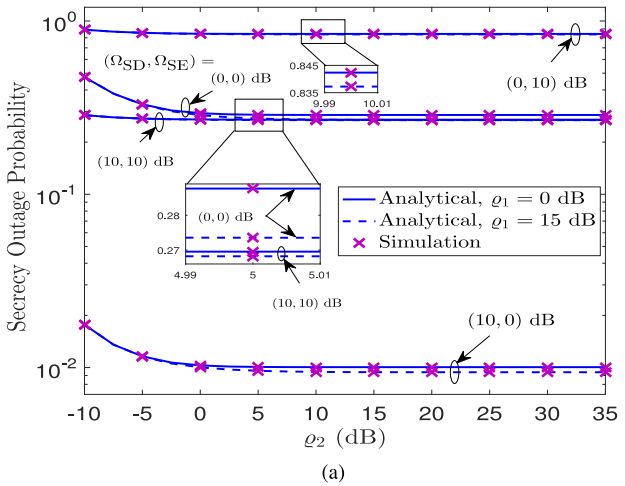

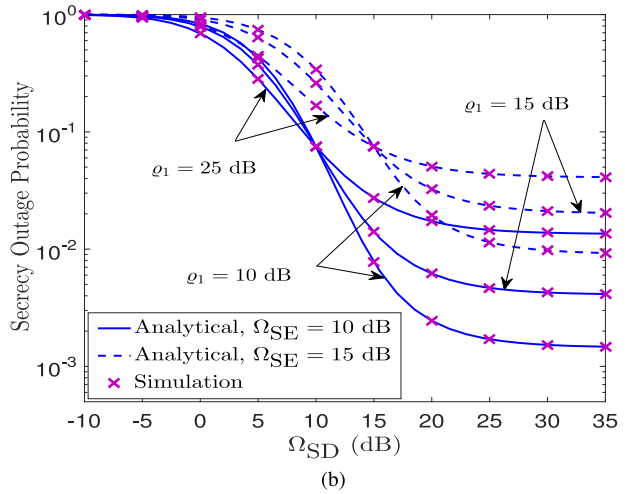

FIGURE 7. SOP versus Ω_{SD} for different values of secondary channels fading severity, N_D, and N_E (a) SOP versus ϱ_2, for several ϱ_1, Ω_{SD}, and Ω_{SE}, and (b) SOP vs Ω_{SD} for different $\varrho_1 = \frac{Q}{N_0}$, under various Ω_{SE}.

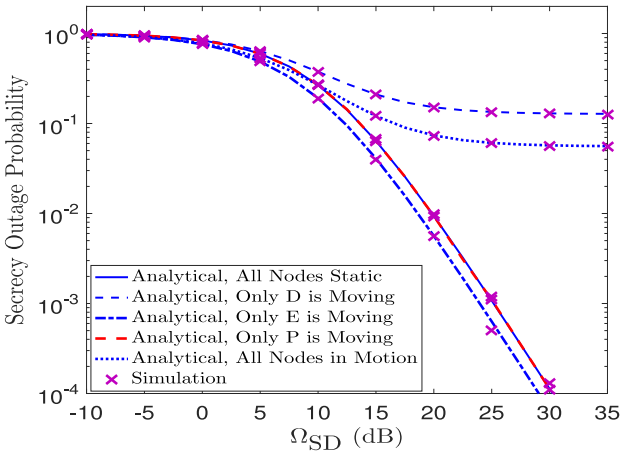

FIGURE 8. SOP performance comparison under various mobility scenarios.

4) IMPACT OF TRANSMIT POWER, INTERFERENCE LIMIT, AND MAIN AND WIRETAP CHANNEL CONDITIONS ON SOP

Fig. 7(a) depicts the SOP versus ϱ_2 (where $\varrho_2 = \frac{P_{\max}}{N_0}$) performance for different interference temperature constraints ϱ_1 and the main channel (Ω_{SD}) and eavesdropper channel (Ω_{SE}) conditions, when $\mathcal{R}_s = 0.1$ bps/Hz, $(m_{SD}, N_D) = (1, 2)$, $(m_{SE}, N_E) = (1, 1)$, $v_{S_J} = 50$ km/h, $\Omega_{\epsilon_{S_J}} = 0.01$, and $\Omega_{e_{S_J}} = 0.1$, $J \in \{D, E, P\}$. We can infer from Fig. 7(a) that the SOP performance becomes independent of the maximum transmit power available at vehicle S in the medium-to-higher regime of ϱ_2, and hence the system's exhibits a zero secrecy diversity order. This indicates that the advantage of having excessive power at secondary source is limited by the interference temperature constraint ϱ_1. The limit imposed by ϱ_1 alongwith the effects of nodes' mobility and imperfect channel estimates cause a secrecy error floor, which is consistent with the observation drawn in *Corollary 2* of Section III-D. Further, it can also be seen that the SOP performance slightly improves with an increase in ϱ_1, since a higher ϱ_1 imposes less stringent interfering constraints on the secondary transmitter power. Moreover, the SOP performance deteriorates as Ω_{SE} increases, since an improvement in Ω_{SE} enhances the eavesdropper's ability to intercept the confidential information. However, as expected, the SOP performance enhances with the improved legitimated channel quality Ω_{SD}.

Fig. 7(b) depicts the SOP performance versus Ω_{SD} for different values of ϱ_1 and Ω_{SE}, when $\mathcal{R}_s = 0.1$ bps/Hz, $(m_{SD}, N_D) = (2, 3)$, $(m_{SE}, N_E) = (2, 1)$, $\varrho_2 = 30$ dB, $v_{S_J} = 50$ km/h, $\Omega_{\epsilon_{S_J}} = 0.01$, and $\Omega_{e_{S_J}} = \Omega_{\epsilon_{S_J}} + \Omega_{S_J}$, for $J \in \{D, E, P\}$. A closer look into the plots of Fig. 7(b) reveals that the quality of main channel (Ω_{SD}) and the quality of eavesdropper channel (Ω_{SE}) determines how the interference temperature constraints, ϱ_1, can affect the SOP performance. We can observe from Fig. 7(b) that a crossover point occurs when $\Omega_{SD} = \Omega_{SE}$, irrespective of the other involved system/channel parameters. Moreover, it can be seen from Fig. 7(b) that when $\Omega_{SD} < \Omega_{SE}$, the SOP performance improves as ϱ_1 increases. On the contrary, when $\Omega_{SD} > \Omega_{SE}$, increasing ϱ_1 degrades the SOP performance. This is due to the fact that when $\Omega_{SD} < \Omega_{SE}$, the ratio $\frac{1+\Lambda_D}{1+\Lambda_E}$ increases as ϱ_1 increases, which reduces the probability associated with the event $\frac{1+\Lambda_D}{1+\Lambda_E} < \eta$, and hence shows an improvement in SOP performance. The converse is true when $\Omega_{SD} > \Omega_{SE}$ with increased ϱ_1.

5) COMPARATIVE STUDY

Fig. 8 illustrates the SOP performance as a function of Ω_{SD} under different mobility scenarios with perfect channel estimation case, when $\mathcal{R}_s = 0.1$ bps/Hz, $(m_{SD}, N_D) = (1, 2)$, $(m_{SE}, N_E) = (1, 1)$, $\varrho_1 = 10$ dB, $\varrho_2 = 30$ dB, $v_{S_J} = 50$ km/h and $\Omega_{\epsilon_{S_J}} = 0$, $J \in \{D, E, P\}$. From Fig. 8, it can be seen that whenever the legitimated link (S $\rightarrow$ D) is subjected to mobility effects, the SOP performance observes a secrecy floor, and thus denying any diversity benefits. For instance from Fig. 8, consider the scenarios; 1) when all the nodes are in motion, and 2) when only D is in motion. The SOP performance is

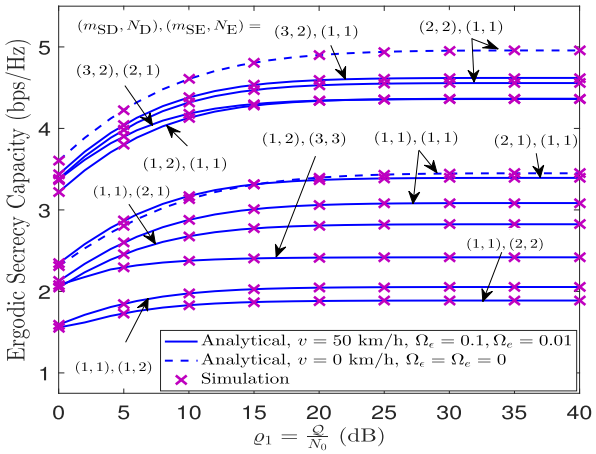

FIGURE 9. Impact of fading severity and multiple antennas on ESC.

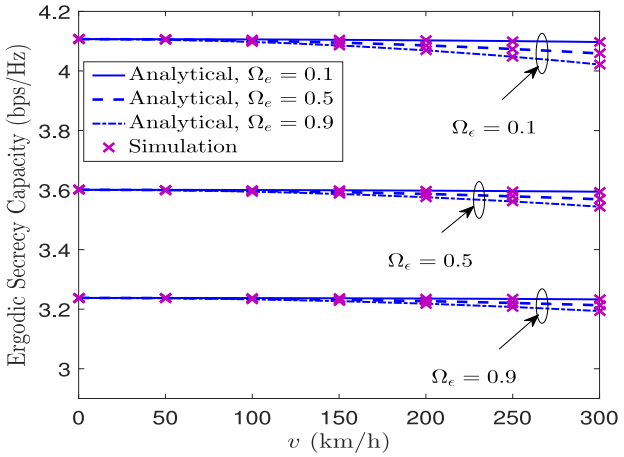

FIGURE 10. ESC versus v for different time varying and channel estimation errors.

poorer under the scenario when D is in motion than that of the case where all the nodes are in motion, since in the former case E is free from the detrimental effects of nodes' mobility which improves its interception capability. Furthermore, we can see that the system observes secrecy diversity benefits for the cases when the channel associated with the destination is free from the mobility effects. Moreover, it is to be noted that the best SOP performance can be achieved for the case when only E is in motion and rest of the nodes are static, even than the case when all the nodes are static. This is due to the reason that E's ability to intercept the information degrades severely because of the errors introduced due to the mobility effect. Also, another interesting observation is that the mobility of primary receiver (when only P is in motion) has negligible impact on the system's SOP performance and also does not affect the system secrecy diversity order.

B. ESC ANALYSIS

Fig 9 illustrates the impact of ϱ_1 on the ESC performance for different values of fading severity parameters (m_{SD}, m_{SE}) and number of antennas N_D and N_E, when $m_{SP} = 1$, $\Omega_{SD} = 10$ dB, $\Omega_{SE} = \Omega_{SP} = 0$ dB, $\varrho_2 = 30$ dB, $v_{Sj} = v = \{0, 50\}$ km/h, $\Omega_e = \Omega_{e_{Sj}} = \{0, 0.01\}$, $\Omega_\epsilon = \Omega_{\epsilon_{Sj}} = \{0, 0.1\}$, for $j \in \{D, E, P\}$). From the different curves in Fig 9, we can see that the derived analytical results are in perfect agreement with the simulation results over the entire range of ϱ_1, which confirms the accuracy of the derived analytical expression for the ESC given in (34). Furthermore, it can be observed that the ESC performance improves in the low-to-medium ϱ_1 regime, and then saturates in the high ϱ_1 regime. This saturation behavior is because of two reasons; 1) simultaneous improvement in ϱ_1 at both the D and E, and 2) joint impact of nodes' mobility and imperfect channel estimates. Moreover, we can infer that as m_{SD} and/or N_D increase, the system's ESC performance improves, since increasing m_{SD} and/or N_D will strengthen the quality of the legitimate link. Whereas, the ESC performance degrades with the increased m_{SE} and/or N_E, since these factors enhance the eavesdropper ability to intercept the confidential

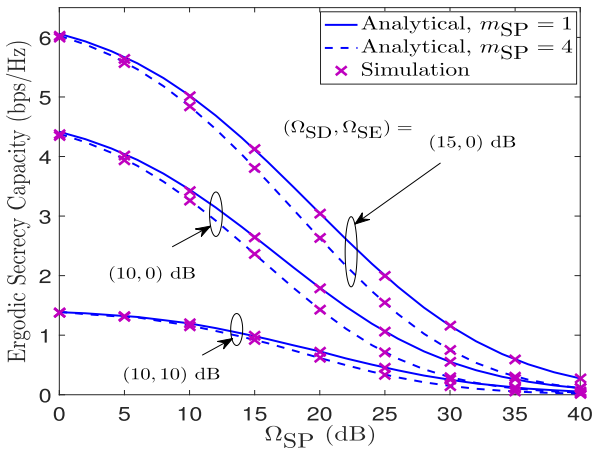

FIGURE 11. Impact of interference channel and secondary channels on ESC.

information. Furthermore, we can infer that N_D and N_E have more dominating impact on the system's ESC performance compared to the fading severity parameters, m_{SD} and m_{SE}. For a fair comparison, we also compare the ESC performance of the considered system in Fig. 9 with the case when all the nodes in the networks are static with perfect channel estimates. In this case ($v = 0$ km/h, $\Omega_e = 0$, and $\Omega_\epsilon = 0$), we can see that the ESC performance improves significantly in comparison of the case $v = 50$ km/h, $\Omega_e = 0.01$, and $\Omega_\epsilon = 0.1$ over the entire range of ϱ_1. However, an error floor in the high ϱ_1 regime will also occur, since ϱ_1 at both D and E improved simultaneously.

Fig. 10 shows the joint impact of nodes' mobility and imperfect channel estimates on the ESC performance when $m_{SD} = m_{SE} = 3$, $m_{SP} = 1$, $N_D = 2$, $N_E = 1$, $\Omega_{SD} = 10$ dB, $\Omega_{SE} = 10$ dB, $\Omega_{SP} = 0$ dB, $\varrho_1 = 10$ dB, and $\varrho_2 = 30$. We also set $v = v_{Sj}, \Omega_e = \Omega_{e_{Sj}}$, and $\Omega_\epsilon = \Omega_{\epsilon_{Sj}}$, for $j \in \{D, E, P\}$). It can be seen from this figure that the ESC performance decreases as v increases, since the likelihood of

the channel to undergo the time-selective fading increases. Moreover, we can observe that the ESC performance reduces as channel estimation error (Ω_ϵ) increases, which further deteriorates with the increased time varying error (Ω_e).

Fig. 11 shows the ESC as a function of interference channel quality Ω_{SP} for various values of m_{SP}, Ω_{SD}, and Ω_{SE}, when $m_{\mathrm{SD}} = m_{\mathrm{SE}} = 1$, $N_{\mathrm{D}} = 2$, $N_{\mathrm{E}} = 1$, $\varrho_1 = 10$ dB, $\varrho_2 = 30$, $v_{\mathrm{S}_J} = 50$ km/h, and $\Omega_{\epsilon_{\mathrm{S}_J}} = 0.01$, and $\Omega_{e_{\mathrm{S}_J}} = 0.1$, for $J \in \{\mathrm{D}, \mathrm{E}, \mathrm{P}\}$. From this figure, we can observe that as Ω_{SP} and/or m_{SP} increase, the ESC becomes poorer for fixed values of Ω_{SD} and Ω_{SE}. This is because of the reason that as Ω_{SP} increases, the interference temperature constraint becomes tight, or in other words, transmit power at the source node reduces. Furthermore, as expected, an increase in the legitimate channel quality (Ω_{SD}) improves the ESC performance, while an increase in wiretap channel quality (Ω_{SE}) degrades the ESC performance.

V. CONCLUSION

This paper investigated the joint impact of nodes' mobility and imperfect channel estimates on the secrecy performance of an underlay CRVN, where in the secondary network, a single-antenna secondary source vehicle wants to transmit its confidential information to the multi-antenna secondary destination vehicle under the availability of a multi-antenna secondary eavesdropper vehicle, in the presence of a primary receiver of primary network. Specifically, by considering combined power constraint of the interference on the primary network and the maximum transmit power constraint on the secondary network, and by taking the impact of nodes' mobility and imperfect channel estimates into account, we deduced the exact SOP and ESC expressions under Nakagami-m fading channels. We also presented the asymptotic SOP analysis to highlight key insights into the system's secrecy diversity order. It was shown that the nodes' mobility and imperfect channel estimates reduce the achievable secrecy diversity order to zero. Furthermore, from the derived expressions, we also discussed several practical cases of interest to have a deeper insights into the system performance behavior. We also presented and quantified the impact of several system/channel parameters on the secrecy performance of the considered system. Finally, we corroborated our theoretical and analytical outcomes via numerical and simulation results.

APPENDIX A
PROOF OF THEOREM 1

From (16), we can have

$$\mathcal{P}^{\mathrm{sec}}_{\mathrm{out},1}(\eta) = \Pr\left[\frac{1+\frac{\varrho_1\rho^2_{\mathrm{SD}}\hat{Y}}{\rho^2_{\mathrm{SP}}\hat{X}+\Omega_{w_{\mathrm{SP}}}+\varrho_1\Omega_{w_{\mathrm{SD}}}}}{1+\frac{\varrho_1\rho^2_{\mathrm{SE}}\hat{Z}}{\rho^2_{\mathrm{SP}}\hat{X}+\Omega_{w_{\mathrm{SP}}}+\varrho_1\Omega_{w_{\mathrm{SE}}}}} < \eta, \hat{X} > c_1\right], \tag{37}$$

where $c_1 = (\frac{\varrho_1}{\varrho_2} - \Omega_{w_{\mathrm{SP}}})\frac{1}{\rho^2_{\mathrm{SP}}}$. Further, after some manipulations, we can express (37) into its equivalent integral form as

$$\mathcal{P}^{\mathrm{sec}}_{\mathrm{out},1}(\eta) = \int_{c_1}^{\infty}\left[\int_0^{\infty} F_{\hat{Y}}\left(\frac{\eta\alpha_2 z(x+\theta_1)}{(x+\theta_2)\alpha_1} + \frac{(\eta-1)(x+\theta_1)}{\varrho_1\alpha_1}\right) \times f_{\hat{Z}}(z)dz\right] f_{\hat{X}}(x)dx. \tag{38}$$

Now, invoking the CDF of $\hat{Y}$ and the PDF of $\hat{Z}$ into the inner integral (say $\mathcal{T}_1(\eta, x)$) of (38), and using the fact that $\Upsilon(n,x) = (n-1)![1 - \mathrm{e}^{-x}\sum_{k=0}^{n-1}\frac{x^k}{k!}]$ [60, eq. (8.352.6)], we can express $\mathcal{T}_1(\eta, x)$ as

$$\mathcal{T}_1(\eta,x) = \frac{\left(\frac{m_{\mathrm{SE}}}{\Omega_{\mathrm{SE}}}\right)^{N_{\mathrm{E}}m_{\mathrm{SE}}}}{\Gamma(N_{\mathrm{E}}m_{\mathrm{SE}})}\left[\mathcal{T}_{11} - \sum_{w=0}^{N_{\mathrm{D}}m_{\mathrm{SD}}-1}\frac{\left(\frac{m_{\mathrm{SD}}}{\Omega_{\mathrm{SD}}}\right)^w}{w!}\mathcal{T}_{12}(\eta,x)\right], \tag{39}$$

where

$$\mathcal{T}_{11} = \int_0^{\infty} z^{N_{\mathrm{E}}m_{\mathrm{SE}}-1}\,\mathrm{e}^{-\frac{m_{\mathrm{SE}}}{\Omega_{\mathrm{SE}}}z}dz. \tag{40}$$

$$\mathcal{T}_{12}(\eta,x) = \mathrm{e}^{-\frac{m_{\mathrm{SD}}}{\Omega_{\mathrm{SD}}}\frac{(\eta-1)(x+\theta_1)}{\varrho_1\alpha_1}}\int_0^{\infty} z^{N_{\mathrm{E}}m_{\mathrm{SE}}-1}\left(\frac{\eta\alpha_2 z(x+\theta_1)}{(x+\theta_2)\alpha_1} + \frac{(\eta-1)(x+\theta_1)}{\varrho_1\alpha_1}\right)^w \mathrm{e}^{-\left(\frac{m_{\mathrm{SD}}\eta\alpha_2(x+\theta_1)}{\Omega_{\mathrm{SD}}(x+\theta_2)\alpha_1}+\frac{m_{\mathrm{SE}}}{\Omega_{\mathrm{SE}}}\right)z}dz. \tag{41}$$

Further, with the aid of $\int_0^{\infty} x^n\mathrm{e}^{-ax}dx = \frac{\Gamma(n+1)}{a^{n+1}}$ [60, eq. (3.351.3)], we can easily simplify the integral $\mathcal{T}_{11}$ in (40) as

$$\mathcal{T}_{11} = \frac{\Gamma(N_{\mathrm{E}}m_{\mathrm{SE}})}{\left(\frac{m_{\mathrm{SE}}}{\Omega_{\mathrm{SE}}}\right)^{N_{\mathrm{E}}m_{\mathrm{SE}}}}. \tag{42}$$

Moreover, by applying the fact $(a+x)^n = \sum_{k=0}^{n}\binom{n}{k}x^k a^{n-k}$ [60, eq. (1.111)] into (41), and solving the resultant integral via [60, eq. (3.351.3)], we can express $\mathcal{T}_{12}(\eta, x)$ in (41) as

$$\mathcal{T}_{12}(\eta,x) = \sum_{u_1=0}^{w}\binom{w}{u_1}\left(\frac{\eta-1}{\varrho_1}\right)^{w-u_1}\frac{(\eta\alpha_2)^{u_1}}{\alpha_1^w}\frac{(x+\theta_1)^w}{(x+\theta_2)^{u_1}} \times \mathrm{e}^{-\frac{m_{\mathrm{SD}}}{\Omega_{\mathrm{SD}}}\frac{(\eta-1)(x+\theta_1)}{\varrho_1\alpha_1}}\frac{\Gamma(N_{\mathrm{E}}m_{\mathrm{SE}}+u_1)}{\left(\frac{m_{\mathrm{SD}}\eta\alpha_2(x+\theta_1)}{\Omega_{\mathrm{SD}}\alpha_1(x+\theta_2)}+\frac{m_{\mathrm{SE}}}{\Omega_{\mathrm{SE}}}\right)^{N_{\mathrm{E}}m_{\mathrm{SE}}+u_1}}. \tag{43}$$

Finally, invoking $\mathcal{T}_{11}$ from (42) and $\mathcal{T}_{12}(\eta, x)$ from (43) into (39), we can obtain the solution of $\mathcal{T}_1(\eta, x)$ in (39). Consequently, by substituting the resultant expression of $\mathcal{T}_1(\eta, x)$ alongwith the PDF of $\hat{X}$, $\mathcal{P}^{\mathrm{sec}}_{\mathrm{out},1}(\eta)$ in (38) can be expressed as (44), shown at the bottom of the next page.

The expression in (44) consists of two integrals, i.e., $\mathcal{N}_1$ and $\mathcal{N}_2(\eta)$. Now, by applying the simplification $\int_{\alpha}^{\infty} g(x)dx = \int_0^{\infty} g(x)dx - \int_0^{\alpha} g(x)dx$, and applying the fact [60, eq. (3.381.1)], we can obtain $\mathcal{N}_1 = 1 - \frac{1}{\Gamma(m_{\mathrm{SP}})}\Upsilon(m_{\mathrm{SP}}, \frac{c_1 m_{\mathrm{SP}}}{\Omega_{\mathrm{SP}}})$.

Furthermore, to obtain the solution for $\mathcal{N}_2(\eta)$ in (44), we first use the change of variables $x - c_1 = t$, and then apply the identity $(a+x)^n = \sum_{k=0}^{n}\binom{n}{k}x^k a^{n-k}$ [60, eq. (1.111)] into $\mathcal{N}_2(\eta)$. Consequently, the resultant integral

obtained for $\mathcal{N}_2(\eta)$ can easily be solved with the aid of the fact $\int_0^\infty \frac{x^u e^{-sx}}{(x+\gamma)^v} dx = \Gamma(u+1)\gamma^{u-v+1}\Psi(u+1, u-v+2; s\gamma)$ [62, eq. (2.3.6.9)]. Finally, invoking the obtained solutions for $\mathcal{N}_1$ and $\mathcal{N}_2(\eta)$ into (44), we can obtain $\mathcal{P}^{\text{sec}}_{\text{out},1}(\eta)$ as shown in (18).

Also, using (16), we can express $\mathcal{P}^{\text{sec}}_{\text{out},2}(\eta)$ as

$$\mathcal{P}^{\text{sec}}_{\text{out},2}(\eta) = \underbrace{\Pr\left[\frac{1+\frac{\varrho_2\rho_{\text{SD}}^2\hat{Y}}{\varrho_2\Omega_{w_{\text{SD}}}+1}}{1+\frac{\varrho_2\rho_{\text{SE}}^2\hat{Z}}{\varrho_2\Omega_{w_{\text{SE}}}+1}} < \eta\right]}_{\triangleq \mathcal{S}(\eta)} \frac{\Upsilon\left(m_{\text{SP}}, \frac{m_{\text{SP}}}{\Omega_{\text{SP}}}c_1\right)}{\Gamma(m_{\text{SP}})}. \quad (45)$$

Now, by expressing $\mathcal{S}(\eta)$ in (45) into its equivalent integral form, we can have

$$\mathcal{S}(\eta) = \int_0^\infty F_{\hat{Y}}\left(\frac{(\eta-1)\xi_1}{\varrho_2\rho_{\text{SD}}^2} + \frac{\eta\alpha_2\xi_1 z}{\xi_2\alpha_1}\right) f_{\hat{Z}}(z)dz. \quad (46)$$

By invoking the CDF of $\hat{Y}$ and the PDF of $\hat{Z}$ into (46) and then simplifying via $\Upsilon(n,x) = (n-1)![1-\text{e}^{-x}\sum_{k=0}^{n-1}\frac{x^k}{k!}]$ [60, eq. (8.352.6)], we can express $\mathcal{S}(\eta)$ in (46) as

$$\begin{aligned}\mathcal{S}(\eta) = \frac{1}{\Gamma(N_{\text{E}}m_{\text{SE}})}\left(\frac{m_{\text{SE}}}{\Omega_{\text{SE}}}\right)^{N_{\text{E}}m_{\text{SE}}}\Bigg[\int_0^\infty z^{N_{\text{E}}m_{\text{SE}}-1}\text{e}^{-\frac{m_{\text{SE}}}{\Omega_{\text{SE}}}z}dz \\ - \sum_{m=0}^{N_{\text{D}}m_{\text{SD}}-1}\left(\frac{m_{\text{SD}}}{\Omega_{\text{SD}}}\right)^m\frac{1}{m!}\text{e}^{-\frac{m_{\text{SD}}(\eta-1)\xi_1}{\Omega_{\text{SD}}\varrho_2\rho_{\text{SD}}^2}}\int_0^\infty z^{N_{\text{E}}m_{\text{SE}}-1} \\ \times\left[\frac{(\eta-1)\xi_1}{\varrho_2\rho_{\text{SD}}^2} + \frac{\eta\alpha_2\xi_1 z}{\xi_2\alpha_1}\right]^m\text{e}^{-\left(\frac{m_{\text{SD}}\eta\alpha_2\xi_1}{\Omega_{\text{SD}}\alpha_1\xi_2}+\frac{m_{\text{SE}}}{\Omega_{\text{SE}}}\right)z}dz\Bigg],\end{aligned} \quad (47)$$

where the first integral in (47) can easily be simplified by the use of the fact $\int_0^\infty x^n\text{e}^{-ax}dx = \frac{\Gamma(n+1)}{a^{n+1}}$ [60, eq. (3.351.3)]. Moreover, to obtain the solution for the second integral in (47), we first apply binomial expansion for $[\frac{(\eta-1)\xi_1}{\varrho_2\rho_{\text{SD}}^2} + \frac{\eta\alpha_2\xi_1 z}{\xi_2\alpha_1}]^m$, and then using the identity $\int_0^\infty x^n\text{e}^{-ax}dx = \frac{\Gamma(n+1)}{a^{n+1}}$ [60, eq. (3.351.3)], we can evaluate the second integral of $\mathcal{S}(\eta)$ in (47). Consequently, invoking the resultant solution of $\mathcal{S}(\eta)$ into (45), we can obtain $\mathcal{P}^{\text{sec}}_{\text{out},2}(\eta)$, as shown in (19).

APPENDIX B
PROOF OF THEOREM 2

By defining the variance of time varying error as $\Omega_{e_{\text{S}_J}} = \Omega_{\epsilon_{\text{S}_J}} + \Omega_{\text{S}_J}$, for $J \in \{\text{D}, \text{E}, \text{P}\}$, we can express (16) under the case when $\Omega_{\text{SD}} \to \infty$ with fixed Ω_{SE} as

$$\begin{aligned}\tilde{\mathcal{P}}^{\text{sec,I}}_{\text{out}}(\eta) = \underbrace{\Pr\left[\frac{1+\frac{\alpha_{\text{SD}}}{\Omega_{\text{SD}}}\hat{Y}}{1+\frac{\varrho_1\rho_{\text{SE}}^2\hat{Z}}{\rho_{\text{SP}}^2\hat{X}+\Omega_{w_{\text{SP}}}+\varrho_1\Omega_{w_{\text{SE}}}}} < \eta, \hat{X} > c_1\right]}_{\triangleq \zeta_1(\eta)} \\ + \underbrace{\Pr\left[\frac{1+\frac{\alpha_{\text{SD}}}{\Omega_{\text{SD}}}\hat{Y}}{1+\frac{\varrho_2\rho_{\text{SE}}^2\hat{Z}}{\varrho_2\Omega_{w_{\text{SE}}}+1}} < \eta\right]\Pr\left[\hat{X} < c_1\right]}_{\triangleq \zeta_2(\eta)}.\end{aligned} \quad (48)$$

From (48), we can express $\zeta_1(\eta)$ and $\zeta_2(\eta)$ into their equivalent integral forms, respectively, as

$$\begin{aligned}\zeta_1(\eta) = \int_{c_1}^\infty\int_0^\infty F_{\hat{Y}}\left(\frac{\Omega_{\text{SD}}\eta\alpha_2\varrho_1 z}{(x+\theta_2)\alpha_{\text{SD}}} + \frac{(\eta-1)\Omega_{\text{SD}}}{\alpha_{\text{SD}}}\right) \\ \times f_{\hat{Z}}(z)dz f_{\hat{X}}(x)dx,\end{aligned} \quad (49)$$

$$\zeta_2(\eta) = \int_0^\infty F_{\hat{Y}}\left(\frac{\Omega_{\text{SD}}\eta\varrho_2\rho_{\text{SE}}^2 z}{\xi_2\alpha_{\text{SD}}} + \frac{(\eta-1)\Omega_{\text{SD}}}{\alpha_{\text{SD}}}\right) f_{\hat{Z}}(z)dz. \quad (50)$$

By following the similar steps as adopted to evaluate $\mathcal{P}^{\text{sec}}_{\text{out},1}(\eta)$ in Appendix A, we can easily obtain $\zeta_1(\eta)$. Likewise, we can obtain $\zeta_2(\eta)$ in the similar way as used to evaluate $\mathcal{P}^{\text{sec}}_{\text{out},2}(\eta)$ in Appendix A. Invoking the results for $\zeta_1(\eta)$ and $\zeta_2(\eta)$ into (48), we can express $\tilde{\mathcal{P}}^{\text{sec,I}}_{\text{out}}(\eta)$ as shown in (21).

APPENDIX C
PROOF OF THEOREM 3

By using the relation $\Omega_{e_{\text{S}_J}} = \Omega_{\epsilon_{\text{S}_J}} + \Omega_{\text{S}_J}$, for $J \in \{\text{D}, \text{E}, \text{P}\}$, under the scenario when $\Omega_{\text{SD}}, \Omega_{\text{SE}} \to \infty$, we can obtain the instantaneous SNRs at terminals D and E as $\tilde{\Lambda}_{\text{D}} = \frac{\alpha_{\text{SD}}}{\Omega_{\text{SD}}}\hat{Y}$ and $\tilde{\Lambda}_{\text{E}} = \frac{\alpha_{\text{SE}}}{\Omega_{\text{SE}}}\hat{Z}$, respectively, where $\alpha_{\text{SE}} = \frac{\rho_{\text{SE}}^2}{1-\rho_{\text{SE}}^2}$. Invoking these instantaneous SNRs into (14), we can express the asymptotic

$$\begin{aligned}\mathcal{P}^{\text{sec}}_{\text{out},1}(\eta) = \underbrace{\int_{c_1}^\infty \frac{1}{\Gamma(m_{\text{SP}})}\left(\frac{m_{\text{SP}}}{\Omega_{\text{SP}}}\right)^{m_{\text{SP}}} x^{m_{\text{SP}}-1}\text{e}^{-\frac{m_{\text{SP}}}{\Omega_{\text{SP}}}x}dx}_{\triangleq \mathcal{N}_1} - \frac{1}{\Gamma(N_{\text{E}}m_{\text{SE}})}\left(\frac{m_{\text{SE}}}{\Omega_{\text{SE}}}\right)^{N_{\text{E}}m_{\text{SE}}}\frac{1}{\Gamma(m_{\text{SP}})}\left(\frac{m_{\text{SP}}}{\Omega_{\text{SP}}}\right)^{m_{\text{SP}}} \\ \times\sum_{w=0}^{N_{\text{D}}m_{\text{SD}}-1}\frac{1}{w!}\left(\frac{m_{\text{SD}}}{\Omega_{\text{SD}}}\right)^w\sum_{u_1=0}^{w}\binom{w}{u_1}\left(\frac{\eta-1}{\varrho_1}\right)^{w-u_1}\frac{(\eta\alpha_2)^{u_1}}{\alpha_1^w}\Gamma(N_{\text{E}}m_{\text{SE}}+u_1)\text{e}^{-\left(\frac{m_{\text{SD}}(\eta-1)\theta_1}{\Omega_{\text{SD}}\varrho_1\alpha_1}\right)}\left(\frac{\alpha_1\Omega_{\text{SD}}\Omega_{\text{SE}}}{\beta_1}\right)^{(N_{\text{E}}m_{\text{SE}}+u_1)} \\ \times\underbrace{\int_{c_1}^\infty\frac{(x+\theta_1)^w(x+\theta_2)^{N_{\text{E}}m_{\text{SE}}}}{(x+\frac{\beta_2}{\beta_1})^{N_{\text{E}}m_{\text{SE}}+u_1}}x^{m_{\text{SP}}-1}\text{e}^{-\left[\frac{m_{\text{SD}}(\eta-1)}{\Omega_{\text{SD}}\varrho_1\alpha_1}+\frac{m_{\text{SP}}}{\Omega_{\text{SP}}}\right]x}dx}_{\triangleq \mathcal{N}_2(\eta)}\end{aligned} \quad (44)$$

SOP under this scenario as

$$\tilde{\mathcal{P}}_{\text{out}}^{\text{sec,II}}(\eta) = \Pr\left[\frac{1+\frac{\alpha_{\text{SD}}}{\Omega_{\text{SD}}}\hat{Y}}{1+\frac{\alpha_{\text{SE}}}{\Omega_{\text{SE}}}\hat{Z}} < \eta\right], \tag{51}$$

Further, using some simplifications, we can express (51) as

$$\begin{aligned}\tilde{\mathcal{P}}_{\text{out}}^{\text{sec,II}}(\eta) &= \int_0^\infty F_{\hat{Y}}\left(\frac{(\eta-1)\Omega_{\text{SD}}}{\alpha_{\text{SD}}} + \frac{\eta\Omega_{\text{SD}}\alpha_{\text{SE}}}{\Omega_{\text{SE}}\alpha_{\text{SD}}}z\right) f_{\hat{Z}}(z)dz \\ &= \frac{1}{\Gamma(N_{\text{D}}m_{\text{SD}})\Gamma(N_{\text{E}}m_{\text{SE}})}\left(\frac{m_{\text{SE}}}{\Omega_{\text{SE}}}\right)^{N_{\text{E}}m_{\text{SE}}} \\ &\quad\times \int_0^\infty \Upsilon\left(N_{\text{D}}m_{\text{SD}}, \frac{(\eta-1)m_{\text{SD}}}{\alpha_{\text{SD}}} + \frac{\eta m_{\text{SD}}\alpha_{\text{SE}}}{\Omega_{\text{SE}}\alpha_{\text{SD}}}z\right) \\ &\quad\times z^{N_{\text{E}}m_{\text{SE}}-1}\mathrm{e}^{-\frac{m_{\text{SE}}}{\Omega_{\text{SE}}}z}dz. \end{aligned} \tag{52}$$

Then, by the use of [60, eq. (8.352.6)] and [60, eq. (1.111)], we can express $\tilde{\mathcal{P}}_{\text{out}}^{\text{sec,II}}(\eta)$ in (52) as

$$\begin{aligned}\tilde{\mathcal{P}}_{\text{out}}^{\text{sec,II}}(\eta) &= \frac{\left(\frac{m_{\text{SE}}}{\Omega_{\text{SE}}}\right)^{N_{\text{E}}m_{\text{SE}}}}{\Gamma(N_{\text{E}}m_{\text{SE}})}\Bigg[\int_0^\infty z^{N_{\text{E}}m_{\text{SE}}-1}\mathrm{e}^{-\frac{m_{\text{SE}}}{\Omega_{\text{SE}}}z}dz \\ &\quad - \sum_{b_1=0}^{N_{\text{D}}m_{\text{SD}}-1}\sum_{b_2=0}^{b_1}\frac{1}{b_1!}\binom{b_1}{b_2}(\eta-1)^{b_1-b_2}\left(\frac{m_{\text{SD}}}{\alpha_{\text{SD}}}\right)^{b_1}\left(\frac{\eta\alpha_{\text{SE}}}{\Omega_{\text{SE}}}\right)^{b_2} \\ &\quad\times \mathrm{e}^{-\frac{(\eta-1)m_{\text{SD}}}{\alpha_{\text{SD}}}}\int_0^\infty z^{N_{\text{E}}m_{\text{SE}}+b_2-1}\mathrm{e}^{-\left(\frac{m_{\text{SE}}}{\Omega_{\text{SE}}}+\frac{\eta\alpha_{\text{SE}}m_{\text{SD}}}{\alpha_{\text{SD}}\Omega_{\text{SE}}}\right)z}dz\Bigg], \end{aligned} \tag{53}$$

where both the integrals in (53) can be simplified via $\int_0^\infty x^n\mathrm{e}^{-ax}dx = \frac{\Gamma(n+1)}{a^{n+1}}$ [60, eq. (3.351.3)], and consequently, after some simplifications, the asymptotic SOP under Scenario II can be obtained as given in (24).

APPENDIX D
PROOF OF COROLLARY 1

When $\mathcal{Q} = \kappa P_{\max}$ and $P_{\max} \to \infty$, we have $\varrho_1 = \varrho_2 \to \infty$. Consequently, the instantaneous end-to-end SNRs at D and E given by (12) and (13) reduces to $\Lambda_{\text{D}} \approx \frac{\rho_{\text{SD}}^2}{\Omega_{w_{\text{SD}}}}\hat{Y}$ and $\Lambda_{\text{E}} \approx \frac{\rho_{\text{SE}}^2}{\Omega_{w_{\text{SE}}}}\hat{Z}$, respectively. Further, invoking these reduced SNRs into (14), and after some simplification, we can get $\mathcal{P}_{\text{out}}^{\text{sec,C1}}(\eta) \approx \int_0^\infty F_{\hat{Y}}(\frac{(\eta-1)\Omega_{w_{\text{SD}}}}{\rho_{\text{SD}}^2} + \frac{\eta\rho_{\text{SE}}^2\Omega_{w_{\text{SD}}}}{\rho_{\text{SD}}^2\Omega_{w_{\text{SE}}}})f_{\hat{Z}}(z)dz$. Now, invoking the required CDF and PDF, and carying out the necessary integral, we can express the closed-form expression for $\mathcal{P}_{\text{out}}^{\text{sec,C1}}(\eta)$, when $P_{\max} \to \infty$ as shown in (29).

APPENDIX E
PROOF OF COROLLARY 2

Herein $P_{\max} \to \infty$ which implies $\varrho_2 \to \infty$, and $\mathcal{Q}$ assumes some fixed finite constant value (i.e., ϱ_1 is fixed). Therefore, from (11) we can have $P_{\text{S}} = \min\left(\frac{\mathcal{Q}}{\rho_{\text{SP}}^2|\hat{h}_{\text{SP}}|^2+\Omega_{w_{SP}}}, P_{\max}\right) \approx \frac{\mathcal{Q}}{\rho_{\text{SP}}^2|\hat{h}_{\text{SP}}|^2+\Omega_{w_{SP}}}$. Consequently, we have $\Lambda_{\text{D}} \approx \frac{\varrho_1\rho_{\text{SD}}^2\hat{Y}}{\rho_{\text{SP}}^2\hat{X}+\Omega_{w_{\text{SP}}}+\varrho_1\Omega_{w_{\text{SD}}}}$ and $\Lambda_{\text{E}} \approx \frac{\varrho_1\rho_{\text{SE}}^2\hat{Z}}{\rho_{\text{SP}}^2\hat{X}+\Omega_{w_{\text{SP}}}+\varrho_1\Omega_{w_{\text{SE}}}}$. Invoking these new SNRs into (14), we obtain

$$\tilde{\mathcal{P}}_{\text{out}}^{\text{sec,C2}}(\eta) = \int_0^\infty \mathcal{L}_1(\eta,x)f_{\hat{X}}(x)dx, \tag{54}$$

where $\mathcal{L}_1(\eta,x) = \int_0^\infty F_{\hat{Y}}(\frac{(\eta-1)(x+\theta_1)}{\alpha_1\varrho_1} + \frac{\eta(x+\theta_1)\alpha_2}{\alpha_1(x+\theta_2)}z)f_{\hat{Z}}(z)dz$, and its solution can be obtained by invoking the CDF of $\hat{Y}$ and PDF of $\hat{Z}$, and simplifying by following the same steps as used to obtain (39) in Appendix A. Consequently, invoking the result of $\mathcal{L}_1(\eta,x)$ alongwith the PDF of $\hat{X}$ into (54), and then solving the resultant integral by first using the fact $(a+x)^n = \sum_{k=0}^n\binom{n}{k}x^k a^{n-k}$ [60, eq. (1.111)], and then applying $\int_0^\infty \frac{x^u e^{-sx}}{(x+\gamma)^v}dx = \Gamma(u+1)\gamma^{u-v+1}\Psi(u+1, u-v+2; s\gamma)$ [62, eq. (2.3.6.9)], to obtain (30).

APPENDIX F
PROOF OF THEOREM 3

From (33), we can express $\overline{\mathbb{C}}_{\text{sec},1}$ into its equivalent integral form as

$$\begin{aligned}\overline{\mathbb{C}}_{\text{sec},1} &= \int_{c_1}^\infty \Bigg\{\left(\frac{x+\theta_1}{\varrho_1\alpha_1}\right) \\ &\quad\times \int_0^\infty \ln(1+y)f_{\hat{Y}}\left(\frac{x+\theta_1}{\varrho_1\alpha_1}y\right)F_{\hat{Z}}\left(\frac{x+\theta_1}{\varrho_1\alpha_1}y\right)dy \\ &\quad+\left(\frac{x+\theta_2}{\varrho_1\alpha_2}\right)\int_0^\infty \ln(1+y)F_{\hat{Y}}\left(\frac{x+\theta_2}{\varrho_1\alpha_2}y\right)f_{\hat{Z}}\left(\frac{x+\theta_2}{\varrho_1\alpha_2}y\right)dy \\ &\quad-\left(\frac{x+\theta_2}{\varrho_1\alpha_2}\right)\int_0^\infty \ln(1+y)f_{\hat{Z}}\left(\frac{x+\theta_2}{\varrho_1\alpha_2}y\right)dy\Bigg\}f_{\hat{X}}(x)dx. \end{aligned} \tag{55}$$

Now, invoking the required CDFs and the PDFs into the first, second, and the third inner integrals of (55), and applying the fact $\Upsilon(n,x) = (n-1)![1-\mathrm{e}^{-x}\sum_{k=0}^{n-1}\frac{x^k}{k!}]$ [60, eq. (8.352.6)], and further with some manipulations, we can express (55) as

$$\begin{aligned}\overline{\mathbb{C}}_{\text{sec},1} &= \int_{c_1}^\infty \Bigg\{\frac{\left(\frac{m_{\text{SD}}}{\Omega_{\text{SD}}}\right)^{N_{\text{D}}m_{\text{SD}}}}{\Gamma(N_{\text{D}}m_{\text{SD}})}\left(\frac{x+\theta_1}{\varrho_1\alpha_1}\right)^{N_{\text{D}}m_{\text{SD}}} \\ &\quad\times\Bigg[\underbrace{\int_0^\infty \ln(1+y)y^{N_{\text{D}}m_{\text{SD}}-1}\mathrm{e}^{-\tau_1(x+\theta_1)y}dy}_{\triangleq\mathcal{I}_1(x)} - \sum_{n_1=0}^{N_{\text{E}}m_{\text{SE}}-1}\frac{\left(\frac{m_{\text{SE}}}{\Omega_{\text{SE}}}\right)^{n_1}}{n_1!} \\ &\quad\times\left(\frac{x+\theta_1}{\varrho_1\alpha_1}\right)^{n_1}\underbrace{\int_0^\infty \ln(1+y)y^{N_{\text{D}}m_{\text{SD}}+n_1-1}\mathrm{e}^{-\tau_2(x+\theta_1)y}dy}_{\triangleq\mathcal{I}_2(x)}\Bigg] \\ &\quad-\frac{\left(\frac{m_{\text{SE}}}{\Omega_{\text{SE}}}\right)^{N_{\text{E}}m_{\text{SE}}}}{\Gamma(N_{\text{E}}m_{\text{SE}})}\sum_{n_2=0}^{N_{\text{D}}m_{\text{SD}}-1}\frac{\left(\frac{m_{\text{SD}}}{\Omega_{\text{SD}}}\right)^{n_2}}{n_2!}\left(\frac{x+\theta_2}{\varrho_1\alpha_2}\right)^{N_{\text{E}}m_{\text{SE}}+n_2} \end{aligned}$$

$$\times \underbrace{\int_0^{\infty} \ln(1+y) y^{N_{\mathrm{E}} m_{\mathrm{SE}}+n_2-1} \mathrm{e}^{-\bar{\tau}_2(x+\theta_2)y} dy}_{\triangleq \mathcal{I}_3(x)} \Bigg\} f_{\hat{X}}(x) dx. \tag{56}$$

The integral $\mathcal{I}_1(x)$ can be solved with the facts $\ln(1+y) = \mathcal{G}_{2,2}^{1,2}(y|_{1,0}^{1,1})$ [63, eq. (8.4.6.5)] and [60, eq. (7.813.1)] as

$$\mathcal{I}_1(x) = \left(\frac{m_{\mathrm{SD}}}{\Omega_{\mathrm{SD}}}\left(\frac{x+\theta_1}{\varrho_1 \alpha_1}\right)\right)^{-N_{\mathrm{D}} m_{\mathrm{SD}}} \times \mathcal{G}_{3,2}^{1,3}\left(\frac{1}{(x+\theta_1)\tau_1}\Bigg|_{1,0}^{1-N_{\mathrm{D}} m_{\mathrm{SD}},1,1}\right). \tag{57}$$

Likewise, we can obtain the solutions for both the remaining integrals, $\mathcal{I}_2(x)$ and $\mathcal{I}_3(x)$, respectively, as

$$\mathcal{I}_2(x) = \left(\frac{m_{\mathrm{SD}}}{\Omega_{\mathrm{SD}}} + \frac{m_{\mathrm{SE}}}{\Omega_{\mathrm{SE}}}\right)^{-N_{\mathrm{D}} m_{\mathrm{SD}}-n_1} \left(\frac{x+\theta_1}{\varrho_1 \alpha_1}\right)^{-N_{\mathrm{D}} m_{\mathrm{SD}}-n_1} \times \mathcal{G}_{3,2}^{1,3}\left(\frac{1}{(x+\theta_1)\tau_2}\Bigg|_{1,0}^{1-N_{\mathrm{D}} m_{\mathrm{SD}}-n_1,1,1}\right), \tag{58}$$

$$\mathcal{I}_3(x) = \left(\frac{m_{\mathrm{SD}}}{\Omega_{\mathrm{SD}}} + \frac{m_{\mathrm{SE}}}{\Omega_{\mathrm{SE}}}\right)^{-N_{\mathrm{E}} m_{\mathrm{SE}}-n_2} \left(\frac{x+\theta_2}{\varrho_1 \alpha_2}\right)^{-N_{\mathrm{E}} m_{\mathrm{SE}}-n_2} \times \mathcal{G}_{3,2}^{1,3}\left(\frac{1}{(x+\theta_2)\tilde{\tau}_2}\Bigg|_{1,0}^{1-N_{\mathrm{E}} m_{\mathrm{SE}}-n_2,1,1}\right). \tag{59}$$

Invoking (57), (58), and (59) into (56) and then applying the fact $\mathcal{G}_{p,q}^{m,n}\left(y\Big|_{b_q}^{a_p}\right) = \mathcal{G}_{q,p}^{n,m}\left(y\Big|_{1-a_p}^{1-b_q}\right)$ [60, eq. (9.31.2)], followed by the change of variables $x - c_1 = t$, we can obtain $\overline{\mathbb{C}}_{\mathrm{sec},1}$ as given in (60), shown at the bottom of the page.

Now, we apply the fact $(a+x)^n = \sum_{k=0}^{n} \binom{n}{k} x^k a^{n-k}$ [60, eq. (1.111)] followed by the substitution $\tau_1 t = x$ into the integral $\mathcal{M}_1$ of (60). Consequently, $\mathcal{M}_1$ can be expressed as

$$\mathcal{M}_1 = \sum_{n_3=0}^{m_{\mathrm{SP}}-1} \binom{m_{\mathrm{SP}}-1}{n_3} c_1^{m_{\mathrm{SP}}-1-n_3} \left(\frac{1}{\tau_1}\right)^{n_3+1} \times \int_0^{\infty} \mathcal{G}_{2,3}^{3,1}\left(x+(\theta_1+c_1)\tau_1\Big|_{N_{\mathrm{D}} m_{\mathrm{SD}},0,0}^{0,1}\right) x^{n_3} \mathrm{e}^{-\frac{m_{\mathrm{SP}}}{\Omega_{\mathrm{SP}}\tau_1}x} dx. \tag{61}$$

The integral in (61) is tedious and intractable, even after applying the fact $\mathrm{e}^{-x} = \mathcal{G}_{0,1}^{1,0}(x|_0^{-})$ [63, eq. (8.4.3.1)]. Therefore, to simplify, we use the Gauss-Laguerre quadrature method [65], and consequently, we can obtain $\mathcal{M}_1$ as

$$\mathcal{M}_1 = \sum_{n_3=0}^{m_{\mathrm{SP}}-1} \binom{m_{\mathrm{SP}}-1}{n_3} c_1^{m_{\mathrm{SP}}-1-n_3} \left(\frac{1}{\tau_1}\right)^{n_3+1} \sum_{i=0}^{N} w_i \times \mathcal{G}_{2,3}^{3,1}\left(x_i+(\theta_1+c_1)\tau_1\Big|_{N_{\mathrm{D}} m_{\mathrm{SD}},0,0}^{0,1}\right) x_i^{n_3} \mathrm{e}^{-\left(\frac{m_{\mathrm{SP}}}{\Omega_{\mathrm{SP}}\tau_1}-1\right)x_i}. \tag{62}$$

Similarly, we can evaluate $\mathcal{M}_2$ and $\mathcal{M}_3$. Consequently, invoking the resultant expressions of $\mathcal{M}_1$, $\mathcal{M}_2$, and $\mathcal{M}_3$ into (60), we can express $\overline{\mathbb{C}}_{\mathrm{sec},1}$ as presented in (35).

Moreover, from (33), we can express $\overline{\mathbb{C}}_{\mathrm{sec},2}$ into its equivalent integral form as

$$\overline{\mathbb{C}}_{\mathrm{sec},2} = \Bigg[\tilde{\xi}_1 \int_0^{\infty} \ln(1+y) f_{\hat{Y}}(\tilde{\xi}_1 y) F_{\hat{Z}}(\tilde{\xi}_1 y) dy + \tilde{\xi}_2 \int_0^{\infty} \ln(1+y) F_{\hat{Y}}(\tilde{\xi}_2 y) f_{\hat{Z}}(\tilde{\xi}_2 y) dy - \tilde{\xi}_2 \int_0^{\infty} \ln(1+y) f_{\hat{Z}}(\tilde{\xi}_2 y) dy \Bigg] F_{\hat{X}}(c_1). \tag{63}$$

Then, invoking the required CDFs and PDFs and after simplifying, $\overline{\mathbb{C}}_{\mathrm{sec},2}$ in (63) can be expressed as (64), shown at the top of the next page. Further, the involved integrals can be evaluated by following the same approach as used to evaluate the integral $\mathcal{I}_1(x)$. Consequently, invoking the obtained solutions to the integrals alongwith the CDF of $\hat{X}$ into (64), we can obtain $\overline{\mathbb{C}}_{\mathrm{sec},2}$ as shown in (36).

$$\overline{\mathbb{C}}_{\mathrm{sec},1} = \left(\frac{m_{\mathrm{SP}}}{\Omega_{\mathrm{SP}}}\right)^{m_{\mathrm{SP}}} \frac{\mathrm{e}^{-\frac{m_{\mathrm{SP}}}{\Omega_{\mathrm{SP}}}c_1}}{\Gamma(m_{\mathrm{SP}})\Gamma(N_{\mathrm{D}} m_{\mathrm{SD}})} \Bigg\{ \underbrace{\int_0^{\infty} \mathcal{G}_{2,3}^{3,1}\left((t+\theta_1+c_1)\tau_1\Big|_{N_{\mathrm{D}} m_{\mathrm{SD}},0,0}^{0,1}\right)(t+c_1)^{m_{\mathrm{SP}}-1} \mathrm{e}^{-\frac{m_{\mathrm{SP}}}{\Omega_{\mathrm{SP}}}t} dt}_{\triangleq \mathcal{M}_1} - \left(\frac{m_{\mathrm{SD}}}{\Omega_{\mathrm{SD}}}\right)^{N_{\mathrm{D}} m_{\mathrm{SD}}} \sum_{n_1=0}^{N_{\mathrm{E}} m_{\mathrm{SE}}-1} \frac{1}{n_1!} \left(\frac{m_{\mathrm{SE}}}{\Omega_{\mathrm{SE}}}\right)^{n_1} \left(\frac{m_{\mathrm{SD}}}{\Omega_{\mathrm{SD}}} + \frac{m_{\mathrm{SE}}}{\Omega_{\mathrm{SE}}}\right)^{-N_{\mathrm{D}} m_{\mathrm{SD}}-n_1} \underbrace{\int_0^{\infty} \mathcal{G}_{2,3}^{3,1}\left((x+\theta_1+c_1)\tau_2\Big|_{N_{\mathrm{D}} m_{\mathrm{SD}}+n_1,0,0}^{0,1}\right)(t+c_1)^{m_{\mathrm{SP}}-1} \mathrm{e}^{-\frac{m_{\mathrm{SP}}}{\Omega_{\mathrm{SP}}}t} dt}_{\triangleq \mathcal{M}_2} \Bigg\} - \left(\frac{m_{\mathrm{SP}}}{\Omega_{\mathrm{SP}}}\right)^{m_{\mathrm{SP}}} \frac{1}{\Gamma(m_{\mathrm{SP}})\Gamma(N_{\mathrm{E}} m_{\mathrm{SE}})} \mathrm{e}^{-\frac{m_{\mathrm{SP}}}{\Omega_{\mathrm{SP}}}c_1} \left(\frac{m_{\mathrm{SE}}}{\Omega_{\mathrm{SE}}}\right)^{N_{\mathrm{E}} m_{\mathrm{SE}}} \sum_{n_2=0}^{N_{\mathrm{D}} m_{\mathrm{SD}}-1} \frac{1}{n_2!} \left(\frac{m_{\mathrm{SD}}}{\Omega_{\mathrm{SD}}}\right)^{n_2} \left(\frac{m_{\mathrm{SE}}}{\Omega_{\mathrm{SE}}} + \frac{m_{\mathrm{SD}}}{\Omega_{\mathrm{SE}}}\right)^{-N_{\mathrm{E}} m_{\mathrm{SE}}-n_2} \times \underbrace{\int_0^{\infty} \mathcal{G}_{2,3}^{3,1}\left((x+\theta_1+c_1)\overline{\tau}_2\Big|_{N_{\mathrm{E}} m_{\mathrm{SE}}+n_2,0,0}^{0,1}\right)(t+c_1)^{m_{\mathrm{SP}}-1} \mathrm{e}^{-\frac{m_{\mathrm{SP}}}{\Omega_{\mathrm{SP}}}t} dt}_{\triangleq \mathcal{M}_3} \tag{60}$$

$$\overline{\mathbb{C}}_{\text{sec},2} = \left\{ \frac{\left(\frac{m_{\text{SD}}\tilde{\xi}_1}{\Omega_{\text{SD}}}\right)^{N_{\text{D}}m_{\text{SD}}}}{\Gamma(N_{\text{D}}m_{\text{SD}})} \left[\int_0^{\infty} \ln(1+y) y^{N_{\text{D}}m_{\text{SD}}-1} \mathrm{e}^{-\frac{m_{\text{SD}}\tilde{\xi}_1}{\Omega_{\text{SD}}}y} dy - \sum_{n_4=0}^{N_{\text{E}}m_{\text{SE}}-1} \frac{\left(\frac{m_{\text{SE}}\tilde{\xi}_1}{\Omega_{\text{SE}}}\right)^{n_4}}{n_4!} \int_0^{\infty} \ln(1+y) y^{N_{\text{D}}m_{\text{SD}}+n_4-1} \right.$$
$$\times \mathrm{e}^{-\left(\frac{m_{\text{SE}}}{\Omega_{\text{SE}}}+\frac{m_{\text{SD}}}{\Omega_{\text{SD}}}\right)\tilde{\xi}_1 y} dy \left. \right] - \left(\frac{m_{\text{SE}}}{\Omega_{\text{SE}}}\right)^{N_{\text{E}}m_{\text{SE}}} \frac{\tilde{\xi}_2^{N_{\text{E}}m_{\text{SE}}}}{\Gamma(N_{\text{E}}m_{\text{SE}})} \sum_{n_5=0}^{N_{\text{D}}m_{\text{SD}}-1} \frac{1}{n_5!} \left(\frac{m_{\text{SD}}\tilde{\xi}_2}{\Omega_{\text{SD}}}\right)^{n_5}$$
$$\times \int_0^{\infty} \ln(1+y) y^{N_{\text{E}}m_{\text{SE}}+n_5-1} \mathrm{e}^{-\left(\frac{m_{\text{SE}}}{\Omega_{\text{SE}}}+\frac{m_{\text{SD}}}{\Omega_{\text{SD}}}\right)\tilde{\xi}_2 y} dy \Bigg\} F_{\hat{X}}(c_1) \tag{64}$$

REFERENCES

[1] B. Ji *et al.*, "Survey on the Internet of Vehicles: Network architectures and applications," *IEEE Commun. Std. Mag.*, vol. 4, no. 1, pp. 34–41, Mar. 2020.

[2] H. Zhou, W. Xu, J. Chen, and W. Weng "Evolutionary V2X technologies toward the Internet of Vehicles: Challenges and opportunities," *Proc. IEEE*, vol. 108, no. 2, pp. 308–320, Feb. 2020.

[3] M. Fallgren, B. Cellarius, M. Dillinger, A. E. Fernandez, Z. Li, and S. Allio, "5GCAR: Executive summary," Dec. 2019. [Online]. Available: https://5gcar.eu/wp-content/uploads/2019/12/5GCAR-Executive-Summary-White-Paper.pdf

[4] V. WS. Wong, R. Schober, D. W. K. Ng, and Li-C. Wang, *Key Technologies for 5G Wireless Systems*. Cambridge, U.K.: Cambridge Univ. Press, 2017.

[5] L. Liang, H. Peng, G. Y. Li, and X. Shen, "Vehicular communications: A physical layer perspective," *IEEE Trans. Veh. Technol.*, vol. 66, no. 12, pp. 10647–10659, Dec. 2017.

[6] Y. Qian, M. Chen, J. Chen, M. S. Hossain, and A. Alamri, "Secure enforcement in cognitive Internet of Vehicles," *IEEE Internet Things J.*, vol. 5, no. 2, pp. 1242–1250, Apr. 2018.

[7] J. Eze, S. Zhang, E. Liu, and E. Eze, "Cognitive radio-enabled Internet of Vehicles: A cooperative spectrum sensing and allocation for vehicular communication," *IET Netw.*, vol. 7, no. 4, pp. 190–199, Jul. 2018.

[8] F. Mehmeti and T. Spyropoulos, "Performance analysis, comparison, and optimization of interweave and underlay spectrum access in cognitive radio networks," *IEEE Trans. Veh. Technol.*, vol. 67, no. 8, pp. 7143–7157, Aug. 2018.

[9] Y. Zou, J. Zhu, L. Yang, Y. Liang, and Y. Yao, "Securing physical-layer communications for cognitive radio networks," *IEEE Commun. Mag.*, vol. 53, no. 9, pp. 48–54, Sep. 2015.

[10] Z. Shu, Y. Qian, and S. Ci, "On physical layer security for cognitive radio networks," *IEEE Netw.*, vol. 27, no. 3, pp. 28–33, Jun. 2013.

[11] Y. Zou, J. Zhu, X. Wang, and L. Hanzo, "A survey on wireless security: Technical challenges, recent advances, and future trends," *Proc. IEEE*, vol. 104, no. 9, pp. 1727–1765, Sep. 2016.

[12] X. Zhou, L. Song, and Y. Zhang, *Physical Layer Security in Wireless Communications*, Boca Raton, FL, USA: CRC Press, 2013.

[13] Y. Zou, X. Wang, and W. Shen, "Optimal relay selection for physical-layer security in cooperative wireless networks," *IEEE J. Sel. Areas Commun.*, vol. 31, no. 10, pp. 2099–2111, Oct. 2013.

[14] L. Fan, N. Yang, T. Q. Duong, M. Elkashlan, and G. K. Karagiannidis, "Exploiting direct links for physical layer security in multiuser multirelay networks," *IEEE Trans. Wireless Commun.*, vol. 15, no. 6, pp. 3856–3867, Jun. 2016.

[15] L. Yang, J. Chen, H. Jiang, S. A. Vorobyov, and H. Zhang, "Optimal relay selection for secure cooperative communications with an adaptive eavesdropper," *IEEE Trans. Wireless Commun.*, vol. 16, no. 1, pp. 26–42, Jan. 2017.

[16] H. Lei, I. S. Ansari, G. Pan, B. Alomair, and M. S. Alouini, "Secrecy capacity analysis over α–μ fading channels," *IEEE Commun. Lett.*, vol. 21, no. 6, pp. 1445–1448, Jun. 2017.

[17] G. C. Alexandropoulos and K. P. Peppas, "Secrecy outage analysis over correlated composite Nakagami-*m*/Gamma fading channels," *IEEE Commun. Lett.*, vol. 22, no. 1, pp. 77–80, Jan. 2018.

[18] K. N. Le and V. N. Q. Bao, "Secrecy under Rayleigh-dual correlated rician fading employing opportunistic relays and an adaptive encoder," *IEEE Trans. Veh. Technol.*, vol. 69, no. 5, pp. 5179–5192, May 2020.

[19] X. Chen, D. W. K. Ng, W. H. Gerstacker, and H. H. Chen, "A survey on multiple-antenna techniques for physical layer security," *IEEE Commun. Surv. Tut.*, vol. 19, no. 2, pp. 1027–1053, Apr.–Jun. 2017.

[20] A. Pandey and S. Yadav, "Physical-layer security for cellular multiuser two-way relaying networks with single and multiple decode-and-forward relays," *Trans. Emerg. Telecommun. Tech.*, vol. 30, no. 12, Dec. 2019, Art. no. e3639.

[21] M. K. Shukla, S. Yadav, and N. Purohit, "Secure transmission in cellular multiuser two-way amplify-and-forward relay networks," *IEEE Trans. Veh. Technol.*, vol. 67, no. 12, pp. 11886–11899, Dec. 2018.

[22] G. Anjos, D. Castanheira, A. Silva, A. Gameiro, M. Gomes, and J. P. Vilela, "Exploiting the reciprocal channel for discrete jamming to secure wireless communications against multiple-antenna eavesdropper," *IEEE Access*, vol. 6, pp. 33410–33420, Jun. 2018.

[23] Y. Zou, X. Li, and Y. Liang, "Secrecy outage and diversity analysis of cognitive radio systems," *IEEE J. Sel. Areas Commun.*, vol. 32, no. 11, pp. 2222–2236, Nov. 2014.

[24] A. Singh, M. R. Bhatnagar, and R. K. Mallik, "Physical layer security of a multiantenna-based CR network with single and multiple primary users," *IEEE Trans. Veh. Technol.*, vol. 66, no. 12, pp. 11011–11022, Dec. 2017.

[25] P. Chakraborty and S. Prakriya, "Secrecy outage performance of a cooperative cognitive relay network," *IEEE Commun. Lett.*, vol. 21, no. 2, pp. 326–329, Feb. 2017.

[26] K. Chopra, R. Bose, and A. Joshi, "Secrecy performance of threshold-based cognitive relay network with diversity combining," *J. Commun. Netw.*, vol. 20, no. 4, pp. 383–395, Aug. 2018.

[27] T. X. Quach, H. Tran, E. Uhlemann, and M. T. Truc, "Secrecy performance of cooperative cognitive radio networks under joint secrecy outage and primary user interference constraints," *IEEE Access*, vol. 8, pp. 18442–18455, Jan. 2020.

[28] R. Zhao, Y. Yuan, L. Fan, and Y.-C. He, "Secrecy performance analysis of cognitive decode-and-forward relay networks in Nakagami-*m* fading channels," *IEEE Trans. Commun.*, vol. 65, no. 2, pp. 549–563, Feb. 2017.

[29] H. Lei *et al.*, "On secrecy outage of relay selection in underlay cognitive radio networks over Nakagami-*m* fading channels," *IEEE Trans. Cogn. Commun. Netw.*, vol. 3, no. 4, pp. 614–627, Dec. 2017.

[30] A. Banerjee and S. P. Maity, "On residual energy maximization in cognitive relay networks with eavesdropping," *IEEE Syst. J.*, vol. 14, no. 4, pp. 3836–3846, Dec. 2019. '

[31] M. Bouabdellah, F. El Bouanani, and M-S. Alouini, "A. PHY layer security analysis of uplink cooperative jamming-based underlay CRNs with multi-eavesdroppers," *IEEE Trans. Cogn. Commun. Netw.*, vol. 6, no. 2, pp. 704–717, Jun. 2020.

[32] P. Chen, J. Ouyang, W. Zhu, M. Lin, A. E. Shafie, and N. Al-Dhahir, "Artificial-noise-aided energy-efficient secure beamforming for multi-eavesdroppers in cognitive radio networks," *IEEE Syst. J.*, vol. 14, no. 3, pp. 3801–3812, Sep. 2020.

[33] S. Timilsina, G. A. A. Baduge, and R. F. Schaefer, "Secure communication in spectrum-sharing massive MIMO systems with active eavesdropping," *IEEE Trans. Cogn. Commun. Netw.*, vol. 4, no. 2, pp. 390–405, Jun. 2018.

[34] B. Li, X. Qi, K. Huang, Z. Fei, F. Zhou, and R. Q. Hu, "Security-reliability tradeoff analysis for cooperative noma in cognitive radio networks," *IEEE Trans. Commun.*, vol. 67, no. 1, pp. 83–96, Jan. 2019.

[35] M. H. Khoshafa, J. M. Moualeu, T. M. N. Ngatched, and M. H. Ahmed, "On the performance of secure underlay cognitive radio networks with energy harvesting and dual-antenna selection," *IEEE Commun. Lett.*, vol. 25, no. 6, pp. 1815–1819, Jun. 2021.
[36] S. Yadav, "Secrecy performance of cognitive radio sensor networks over α–μ fading channels," *IEEE Sensors Lett.*, vol. 4, no. 9, Sep. 2020, Art. no. 6002004.
[37] A. Pandey and S. Yadav, "Physical layer security in cooperative AF relaying networks with direct links over mixed rayleigh and double-rayleigh fading channels," *IEEE Trans. Veh. Technol.*, vol. 67, no. 11, pp. 10615–10630, Nov. 2018.
[38] A. U. Makarfi *et al.*, "Towards physical layer security for Internet of Vehicles: Interference aware modelling," *IEEE Internet Things J.*, vol. 8, no. 1, pp. 443–457, Jan. 2021.
[39] N. Jaiswal and N. Purohit, "Performance of downlink NOMA-enabled vehicular communications over double Rayleigh fading channels," *IET Commun.*, vol. 14, no. 20, pp. 3652–3660, Sep. 2020.
[40] C. Wang, Z. Li, J. Shi, J. Si and D. W. K. Ng, "Physical layer security of vehicular networks: A stochastic geometry approach," in *Proc. IEEE Int. Conf. Commun. Workshops*, Dublin, Ireland, 2020, pp. 1–7.
[41] Y. Ai, M. Cheffena, A. Mathur, and H. Lei, "On physical layer security of double Rayleigh fading channels for vehicular communications," *IEEE Wireless Commun. Lett*, vol. 7, no. 6, pp. 1038–1041, Dec. 2018.
[42] M. Rice *et al.*, "Physical-layer security for vehicle-to-everything networks: Increasing security while maintaining reliable communications," *IEEE Veh. Technol. Mag.*, vol. 15, no. 3, pp. 68–76, Sep. 2020.
[43] A. Pandey and S. Yadav, "Physical layer security in cooperative amplify-and-forward relay networks over mixed nakagami-m and double nakagami-m fading channels: Performance evaluation and optimisation," *IET Commun.*, vol. 14, no. 1, pp. 95–104, Jan. 2020.
[44] J. Tang, H. Wen, H. Song, T. Zhang, and K. Qin, "On the security-reliability and secrecy throughput of random mobile user in Internet of Things," *IEEE Internet Things J.*, vol. 7, no. 10, pp. 10635–10649, Oct. 2020.
[45] J. Tang, M. Dabaghchian, K. Zeng and H. Wen, "Impact of mobility on physical layer security over wireless fading channels," *IEEE Wireless Commun.*, vol. 17, no. 12, pp. 7849–7864, Dec. 2018.
[46] S. Ata and E. Erdogan, "Secrecy outage probability of inter-vehicular cognitive radio networks," *Int. J. Commun. Syst.*, vol. 33, no. 4, Mar. 2020. Art. no. e4244.
[47] S. Kavaiya *et al.*, "On physical layer security over α-η-κ-ν fading for relay based vehicular networks," in *Proc. Int. Conf. Signal Process. Commun.*, Bangalore, India, 2020, pp. 1–5.
[48] A. Pandey, S. Yadav, T. Do, and R. Kharel, "Secrecy performance of cooperative cognitive AF Relaying networks with direct links over mixed Rayleigh and double-rayleigh fading channels," *IEEE Trans. Veh. Technol.*, vol. 69, no. 12, pp. 15095–15112, Dec. 2020.
[49] H. Yu, T. Kim, and H. Jafarkhani, "Wireless secure communication with beamforming and jamming in time-varying wiretap channels," *IEEE Trans. Inf. Forensics Secur.*, vol. 13, no. 8, pp. 2087–2100, Aug. 2018.
[50] Y. Huang, F. S. Al-Qahtani, T. Q. Duong, and J. Wang, "Secure transmission in MIMO wiretap channels using general-order transmit antenna selection with outdated CSI," *IEEE Trans. Commun.*, vol. 63, no. 8, pp. 2959–2971, Aug. 2015.
[51] S. Kavaiya, D. K. Patel, Z. Ding, Y. L. Guan, and S. Sun, "Physical layer security in cognitive vehicular networks," *IEEE Trans. Commun.*, vol. 69, no. 4, pp. 2557–2569, Apr. 2021.
[52] S. Yadav and A. Pandey, "Secrecy performance of cognitive vehicular radio networks: Joint impact of nodes mobility and imperfect channel estimates," in *Proc. IEEE Int. Black Sea Conf. Commun. Netw.*, 2020, pp. 1–7.
[53] F. Tang, Y. Kawamoto, N. Kato, and J. Liu, "Future intelligent and secure vehicular network toward 6G: Machine-learning approaches," *Proc. IEEE*, vol. 108, no. 2, pp. 292–307, Feb. 2020.
[54] Y. M. Khattabi and M. M. Matalgah, "Performance analysis of multiple-relay AF cooperative systems over Rayleigh time-selective fading channels with imperfect channel estimation," *IEEE Trans. Veh. Technol.*, vol. 65, no. 1, pp. 427–434, Jan. 2016.
[55] J. P. Kermoal, L. Schumacher, K. I. Pedersen, P. E. Mogensen, and F. Frederiksen, "A stochastic MIMO radio channel model with experimental validation," *IEEE J. Sel. Areas Commun.*, vol. 20, no. 6, pp. 1211–1226, Aug. 2002.
[56] G. J. Foschini and M. J. Gans, "On limits of wireless communications in a fading environment when using multiple antennas," *Wireless Pers. Commun.*, vol. 6, pp. 311–335, Mar. 1998.
[57] R. He, A. F. Molisch, F. Tufvesson, Z. Zhong, B. Ai, and T. Zhang, "Vehicle-to-vehicle propagation models with large vehicle obstructions," *IEEE Trans. Intell. Trans. Syst.*, vol. 15, no. 5, pp. 2237–2248, Oct. 2014.
[58] A. Tassi, M. Egan, R. J. Piechocki, and A. Nix, "Modeling and design of millimeter-wave networks for highway vehicular communication," *IEEE Trans. Veh. Technol.*, vol. 66, no. 12, pp. 10676–10691, Dec. 2017.
[59] M. Suneya *et al.*, "Fading characteristic modeling of V2V communication at 700 MHz band and the system margin design," in *Proc. 20th ITS World Congr. ITS Jpn.*, 2013, pp. 1–10.
[60] I. S. Gradshteyn and I. M. Ryzhik, *Tables of Integrals, Series, and Products*, 6th ed. New York, NY, USA: Academic, 2000.
[61] A. P. Prudnikov, Y. A. Brychkov, and O. I. Marichev, *Integrals and Series Volume 1: Elementary Functions.* New York, NY, USA: Gordon and Breach Science Publishers, 1986.
[62] A. P. Prudnikov, Y. A. Brychkov, and O. I. Marichev, *Integrals and Series Volume 2: Special Functions*. New York, NY, USA: Gordon and Breach Science Publishers, 1992.
[63] A. P. Prudnikov, Y. A. Brychkov, and O. I. Marichev, *Integrals and Series. Vol. 3, More Special Functions*. London, U.K.: Gordon and Breach Science Publishers, 1986.
[64] *The Wolfram Functions Site*, [Online]. Available: http://functions.wolfram.com/
[65] M. Abromowitz and I. A. Stegun, *Handbook of Mathematical Functions With Formulas, Graphs, and Mathematical Tables*, New York, NY, USA: Dover, 1970.
[66] D. K. Patel *et al.*, "Performance analysis of NOMA in vehicular communications over i.n.i.d nakagami-m fading channels," *IEEE Trans. Wireless Commun.*, to be published, doi: 10.1109/TWC.2021.3073050.

ANSHUL PANDEY (Member, IEEE) received the B.Tech. degree in electronics and communication engineering from the PDPM-Indian Institute of Information Technology Design and Manufacturing, Jabalpur, India, in 2012, the M.Tech. degree in advance networks from the ABV-Indian Institute of Information Technology and Management, Gwalior, India, in 2016, and the Ph.D. degree from the Indian Institute of Information Technology Allahabad, Prayagraj, India. He is currently with Secure Systems Research Centre, Technology Innovation Institute, Abu Dhabi, UAE. His research interests include cooperative relaying for wireless vehicular networks, physical layer security, MIMO communications, and signal processing.

SUNEEL YADAV (Member, IEEE) received the B.Tech. degree in electronics and communication engineering from the Meerut Institute of Engineering and Technology, Meerut, India, in 2008, the M.Tech. degree in digital communications from the ABV-Indian Institute of Information Technology and Management, Gwalior, India, in 2012, and the Ph.D. degree in the discipline of electrical engineering with the Indian Institute of Technology Indore, Indore, India, in 2016. He is currently with the Department of Electronics and Communication Engineering, Indian Institute of Information and Technology Allahabad, Prayagraj, India, as an Assistant Professor. He is a Faculty in-Charge of Mobile and Wireless Networking Laboratory, Indian Institute of Information and Technology Allahabad, Prayagraj, India. He has numerous publications in peer-reviewed journals and conferences. His current research interests include wireless relaying techniques, cooperative communications, cognitive relaying networks, device-to-device communications, reconfigurable intelligent surfaces, signal processing, physical layer security, and MIMO systems. He was also a TPC Member, the Session Chair, the Program Co-Chairs, a Reviewer, for various national and international conferences. He is a Reviewer in a number of international journals, including the IEEE TRANSACTIONS ON VEHICULAR TECHNOLOGY, IEEE COMMUNICATIONS LETTERS, IEEE TRANSACTIONS ON COMMUNICATIONS, IEEE TRANSACTIONS ON INFORMATION FORENSICS AND SECURITY, IEEE SYSTEMS JOURNAL, IEEE ACCESS, IEEE INTERNET OF THINGS JOURNAL, IEEE TRANSACTIONS ON SIGNAL AND INFORMATION PROCESSING OVER NETWORKS, and *Physical Communication*.